J|A|C|S
ARTICLES
Published on Web 04/29/2005

Modeling Rate-Controlling Solvent Effects. The Pericyclic Meisenheimer Rearrangement of *N*-Propargylmorpholine *N*-Oxide

Zoltán Mucsi,*[,†] Anna Szabó,[‡] István Hermecz,[‡] Árpád Kucsman,[†] and Imre G. Csizmadia*[,§,||]

Contribution from the Department of Organic Chemistry, Eötvös Loránd University, Budapest, H-1117, Hungary, Department of Organic Chemistry, Technical and Economical University of Budapest, Budapest, H-1111, Hungary, Department of Chemistry, University of Toronto, Toronto, Ontario, Canada, M5S 3H6, and Department of Chemistry and Chemical Informatics, Faculty of Education, University of Szeged, Szeged, H-6725, Hungary

Received December 26, 2004; E-mail: zoltan_mucsi@freemail.hu; icsizmad@jgytf.u-szeged.hu

Abstract: The activation parameters of the pericyclic Meisenheimer rearrangement and a competitive rearrangement of *N*-propargylmorpholine *N*-oxide were determined by experimental and computational methods. A number of aprotic and protic solvents of different polarities and hydrogen bond-forming abilities and the roles of electron-pair acceptor additives were investigated. The reaction kinetics were followed by means of NMR. In protic solvents, isotope-labeling experiments revealed a novel inverse secondary kinetic isotope effect (k_H/k_D about 0.8) for the rate-determining cyclization step, probably occurring because of a C(sp) → C(sp^2) change in hybridization at the reaction center. In molecular computations at the B3LYP/6-31++G(d,p) level of theory, implicit, explicit, and joint explicit−implicit solvent models were used. The explicit−implicit model and molecular dynamic simulations gave the most accurate results. The components of the rate-controlling solvent effect are discussed, and general equations are proposed for accurate prediction of the solvent-dependent activation parameters.

1. Introduction

1.1. Preamble. In drug research, study of the rates of metabolic processes is essential for the development of drugs with the desired effects. If decomposition of the drug is too fast, the compound cannot express its activity on the receptor; if it is too slow, an overdose may occur. Our aim was a quantitative study, using only theoretical considerations, of the rate-determining step of a metabolically occurring process, the Meisenheimer rearrangement of *N*-propargylmorpholine *N*-oxide. Computed and experimentally determined parameters were compared to validate the theoretical models.

1.2. Background. The accurate prediction of different reaction parameters has been a dream of numerous chemists for many years. Currently, the fascinating improvement of computational tools and methods has made theoretical prediction an affordable, almost routine task. However, despite the accurate ab initio and density functional theory (DFT) methods, many theoretical results deviate considerably from the experimental findings because the chemical environment (effects of solvent molecules, such as hydrogen bonding (HB), self-association, etc.) is not successfully taken into account. In this article, we wish to draw attention to the importance of appropriate chemical modeling.

Solvent effects are complex dynamic processes in which a great number of solvent molecules take part and interact with the solute molecules. A completely correct description of such a system is impossible, but attempts can be made to design the average effect in a static model. The most-preferred methods are based on the different polarizable continuum medium (PCM)[1−4] and conductor-like screening models (COSMO).[5] These implicit solvent models deal only with the solute molecule embedded in the infinite polarizable or nonpolarizable continuum medium. However, the implicit model has been found to be inaccurate in most cases because it does not deal explicitly with the solvent molecules. Relatively few works take the solvent molecules into account appropriately, and they do not reflect the importance of this.[6−14] Later in the article, we present

† Eötvös Loránd University.
‡ Technical and Economical University of Budapest.
§ University of Toronto.
|| University of Szeged.

(1) Cancès, M. T.; Mennucci, B.; Tomasi, J. *J. Chem. Phys.* **1997**, *107*, 3032−3041.
(2) Mennucci, B.; Tomasi, J. *J. Chem. Phys.* **1997**, *106*, 5151−5158.
(3) Mennucci, B.; Cancès, E.; Tomasi, J. *J. Phys. Chem. B* **1997**, *101*, 10506−10517.
(4) Tomasi, J.; Mennucci, B.; Cancès, E. *J. Mol. Struct. (THEOCHEM)* **1999**, *464*, 211−226.
(5) Barone, V.; Cossi, M. *J. Phys. Chem. A* **1995**, *102*, 1995−2001.
(6) Buncel, E.; Stairs R. A.; Wilson, H. *The Role of the Solvent in Chemical Reactions*; Oxford University Press: Oxford, 2003.
(7) (a) Blake, J. F.; Jorgensen, W. L. *J. Am. Chem. Soc.* **1991**, *113*, 7430−7432. (b) Severance D. L.; Jorgensen, W. L. *J. Am. Chem. Soc.* **1992**, *114*, 10966−10968.

Scheme 1. Rearrangements of *N*-Propargylmorpholine *N*-Oxide (**1**)

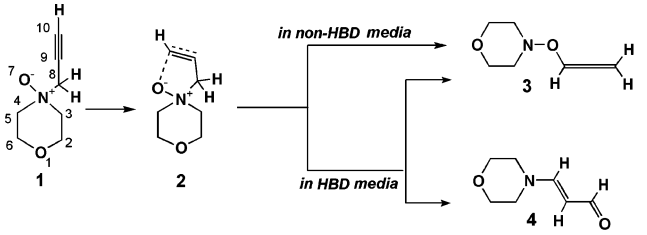

evidence that an explicit consideration of solvent molecules is essential for an acceptable description of chemical processes.

To study the solvent effect, we have chosen the pericyclic Meisenheimer rearrangement of *N*-propargylmorpholine *N*-oxide **1** in different solvents (Scheme 1). In earlier work,[15−17] we demonstrated that both the rate and the product distribution of this pericyclic reaction, which proceeds through a cyclic-activated complex (transition state: TS **2**), are affected by the nature of the solvent. In aprotic solvents (e.g., in diethyl ether) a trisubstituted hydroxylamine, *N*-(propadienyloxy)morpholine (**3**; "O-allenylhydroxylamine" in ref 16) was formed by N−C bond cleavage as a result of the Meisenheimer rearrangement.[18,19] In protic solvents (e.g., in C_1-C_4 alcohols), however, the rate of the Meisenheimer rearrangement was markedly decreased, and in a competitive rearrangement involving N−O cleavage 3-(3-oxapentane-1,5-diyl) aminoacrylaldehyde (**4**; "enamino aldehyde" in ref 16) was formed and became the main component. In C_1-C_4 alcohols, kinetic measurements were performed to determine the rate constants and the activation parameters for both rearrangements.[16] Preliminary theoretical calculations were also carried out to reveal the mechanisms of the competing reaction pathways.[17]

The fact that the rearrangements of *N*-oxide **1**,[18,19] involving a pericyclic rate-determining step, exhibit a significant solvent dependence was unexpected. Most pericyclic reactions that proceed through an isopolar TS (differing in charge separation very little, if at all, from the initial reactant) are not appreciably affected by changes in the substituent or the reaction medium.[20−23] In a few cases, for example, in hetero Diels−Alder reactions, the pericyclic step proceeds markedly faster in hydrogen-bond donor (HBD) solvents than in non-HBD ones,[24−28] and there is

Chart 1. Different Conformations of *N*-Propargylmorpholine *N*-Oxide (**1**)

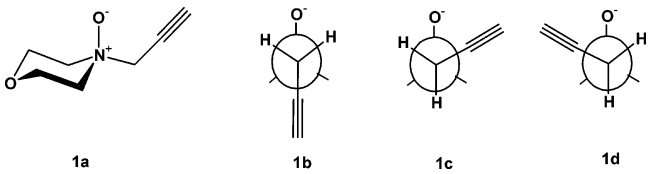

a dramatic rate acceleration when an electron-pair acceptor (EPA) ionophore (e.g., $LiClO_4$ or $NaClO_4$) is added to the reaction mixture.[23,29,30] These results were explained by the enhanced polarity of the TSs, stabilized less effectively by HBD solvents and EPAs, as compared with that in the reactants.

This unexpected solvent effect was a challenge to develop theoretical methods for prediction of the effect of the reaction medium. The Meisenheimer rearrangement of *N*-oxides is additionally of biological importance. In vivo degradation of the excellent irreversible monoamine oxidase (MAO) inhibitors[31,32] (e.g., MAO-A: Clorgyline, Abbott-21.855; MAO-B: Selegiline, Pargyline), essentially tertiary amines with *N*-propargyl and *N*-methyl substituents (for individual structures, see Scheme S1 in the Supporting Information), starts with a Meisenheimer rearrangement of the corresponding *N*-oxides.[15] Furthermore, it has recently been discovered[33] that Selegiline-*N*-oxide is a very strong neuroprotective agent. This discovery is suggestive of the promise of development of a potential new drug.

1.3. Scope. In our present work, we started from the well-established mechanism of the rearrangement of **1** that we proposed earlier.[16,17] To reveal the controlling role of the reaction medium, we carried out the reaction not only in the previously investigated HBD solvents (MeOH, EtOH, *i*-PrOH, and *t*-BuOH), but also in other HBD solvents [H_2O, CF_3CH_2OH, $(CF_3)_2CHOH$, $CHCl_3$, $CHBr_3$, CH_2Cl_2, and $MeNO_2$], in non-HBD solvents (Me_2SO, MeCN, Me_2CO, pyridine, and dioxane), in the presence of electron-pair acceptors (EPAs such as Li^+, Na^+, nitro derivatives of benzene, BF_3:OEt_2 and H^+ interacting with the nonbonding electron pair of the *N*-oxide oxygen), and in deuterated solvents (D_2O, CD_3OD, C_2D_5OD, $CDCl_3$, $CDBr_3$, and CD_2Cl_2).

In the models of solvent effects, the solvents and media are divided into two groups. Type 1 media are non-HBD (aprotic) solvents: Me_2SO, MeCN, Me_2CO, pyridine, dioxane, and vacuum. For appropriate modeling, we divided the type 2 solvents into two subgroups: weak HBD solvents such as $CHCl_3$,[34−37] $CHBr_3$, CH_2Cl_2, and $MeNO_2$ (prominently weak) belong to type 2A, whereas strong HBD solvents such as H_2O, MeOH, EtOH, CF_3CH_2OH, *i*-PrOH, $(CF_3)_2CHOH$, and *t*-BuOH belong to type 2B.[38−40]

(8) Jones-Hertzog, D. K.; Jorgensen, W. L. *J. Am. Chem. Soc.* **1995**, *117*, 9077−9078.
(9) Cossi, M.; Barone, V. *J. Chem. Phys.* **2000**, *112*, 2427−2435.
(10) Cossi, M.; Barone, V. *J. Chem. Phys.* **2001**, *115*, 4708−4717.
(11) Sicinska, D.; Paneth, P.; Truhlar, D. G. *J. Phys. Chem. B* **2002**, *106*, 2708−2713.
(12) Lee, M. R.; Tsai, J.; Baker, D.; Kollman, P. A. *J. Mol. Biol.* **2001**, *313*, 417−430.
(13) Roux, B.; Simonson, T. *Biophys. Chem.* **1999**, *78*, 1−20.
(14) Importa, R.; Scalmi, G.; Barone, V. *Chem. Phys. Lett.* **2001**, *336*, 349−356.
(15) Szabó, A.; Hermecz, I. *J. Org. Chem.* **2001**, *66*, 7219−7222.
(16) Szabó, A.; Galambos-Faragó, A.; Mucsi, Z.; Timári, G.; Vasvári-Debreczy, L.; Hermecz, I. *Eur. J. Org. Chem.* **2004**, 687−694.
(17) Mucsi, Z.; Szabó, A.; Hermecz, I. *J. Mol. Struct. (THEOCHEM)* **2004**, *666−667*, 547−556.
(18) Johnstone, R. A. W. *Mech. Mol. Migr.* **1969**, *2*, 249−266.
(19) Schöllkopf, U.; Patsch, M.; Schäfer, H. *Tetrahedron Lett.* **1964**, *36*, 2515−2520.
(20) Dewar, M. J. S.; Pyron, R. S. *J. Am. Chem. Soc.* **1970**, *92*, 3098−3103.
(21) Harkness, J. B.; Kistiakowsky, G. B.; Mears, W. H. *J. Chem. Phys.* **1937**, *5*, 682−694.
(22) Kaufmann, H.; Wassermann, J. *J. Chem. Soc.* **1939**, 870−871.
(23) Reichardt, C. *Solvents and Solvents Effect in Organic Chemistry*; Wiley-VCH: Weinheim, Germany, 2003; Chapter 5, pp 148−328.
(24) Rideout, D. C.; Breslow, R. *J. Am. Chem. Soc.* **1980**, *102*, 7816−7817.
(25) Breslow, R. *Acc. Chem. Res.* **1991**, *24*, 159−164.
(26) Breslow, R. *Green Chem.* **1998**, 225−233.
(27) Jorgensen, W. L.; Blake, J. F.; Lim, D.; Severance, D. L. *J. Chem. Soc., Faraday Trans.* **1994**, *90*, 1727−1732.
(28) Kumar, A. *Chem. Rev.* **2001**, *101*, 1−19.
(29) Sankararaman, S.; Nesakumar, J. E. *Eur. J Org. Chem.* **2000**, 2003−2011.
(30) Waldmann, H. *Angew. Chem.* **1991**, *103*, 1335−1337.
(31) Abeles, R. H.; Maycock, A. L. *Acc. Chem. Res.* **1976**, *9*, 313−319.
(32) Gaál, J.; Hermecz, I. In *Inhibitors of Monoamine Oxidase B*; Szelényi, I., Ed.; Birkhäuser: Basel, 1999; pp 75−108.
(33) Magyar, K.; Pálfi, M.; Tábi, T.; Kalász, H.; Szende, B.; Szökö, É. *Curr. Med. Chem.* **2004**, *11*, 2017−2031.
(34) Douglas, C.; McHale, J. L. *J. Phys. Chem. A* **1997**, *101*, 3070−3077.
(35) Sauer J.; Prahl, H. *Chem. Ber.* **1969**, *102*, 1917−1927.
(36) Greenwald, R.; Chaykovsky, M.; Corey, E. J. *J. Org. Chem.* **1963**, *28*, 1128−1129.
(37) Domingo, L. R.; Andrés, J. *J. Org. Chem.* **2003**, *68*, 8662−8668.

Scheme 2. Suggested Mechanism for the Rearrangements of *N*-Propargylmorpholine *N*-Oxide (**1**) in Type 1, Type 2A, and Type 2B Solvents[a]

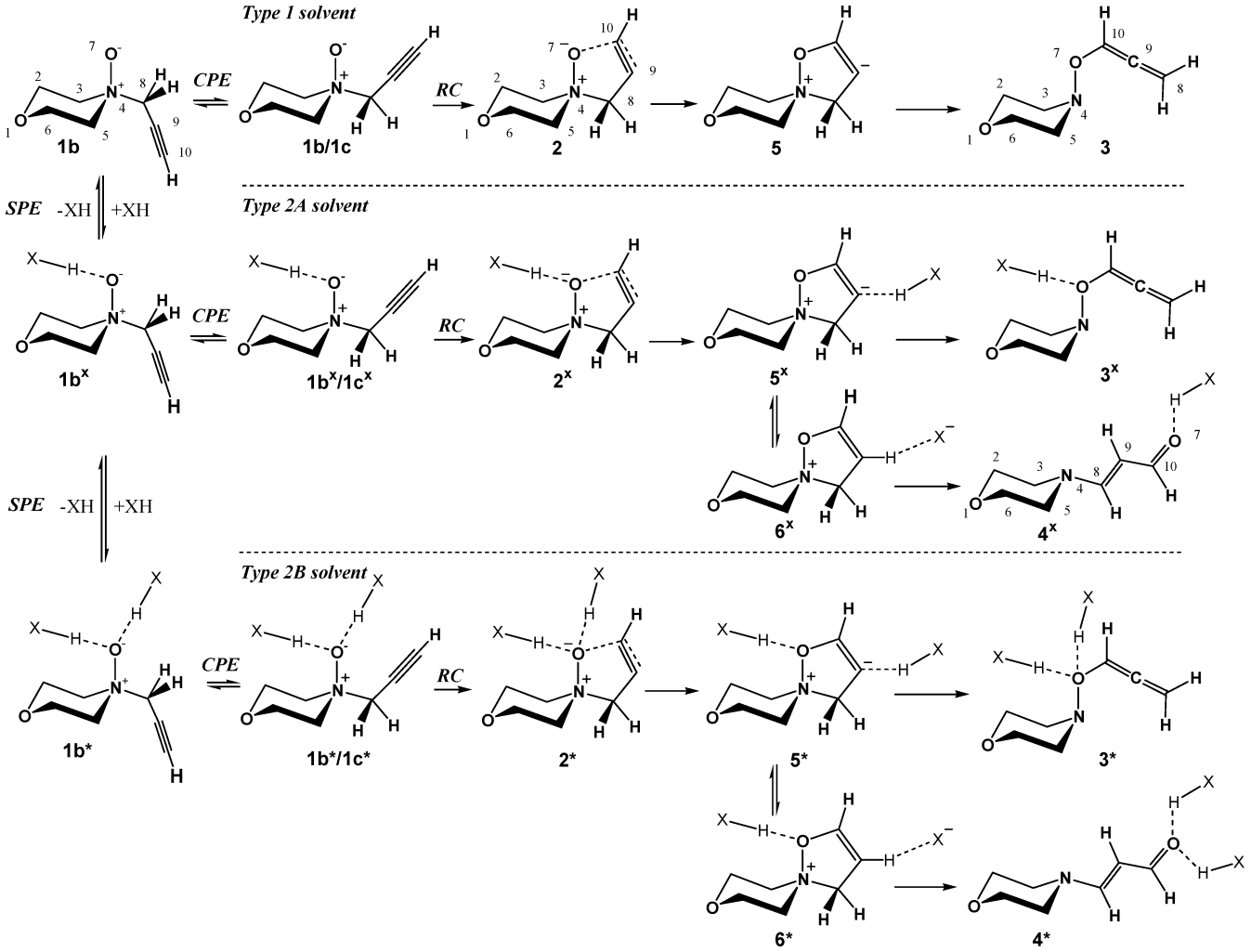

[a] CPE: conformational pre-equilibrium, SPE: solvent−solute pre-equilibrium, RC: ring-closure step, X−H = OH or CH.

The reaction starts with the syn-clinal (gauche, **1c**/**1d**) conformation, even though the anti-periplanar (**1b**) conformation is considerably more stable (Chart 1). The conformational pre-equilibrium (CPE) is illustrated in Scheme 2.[16]

While different PCM methods are effective in providing an adequate model of the effects of type 1 solvents, it is difficult to find an appropriate environmental and chemical model for protic solvents. The question arises of how many solvent molecules should be taken into account. If we focus only on the first solvation shell around the *N*-oxygen of **1**, are one or two or three solvent molecules able to interact with the three nonbonded electron pairs of the negative acceptor oxygen atom?[32−34] We carried out computations on models containing zero or one or two solvent molecules of type 2; for one solvent (MeOH), we also computed the model involving three solvent molecules.

In this article, we compute the Gibbs free energy of the rate-determining step ($\Delta G^{\ddagger}_{TOT}$; see Section 3.3) and compare it with the experimentally determined value ($\Delta G^{\ddagger}_{OBS}$). Equations 1−6 reveal the components of the experimentally determined Gibbs free energies of activation of the processes shown in Scheme 2 and the associated thermodynamic levels.

In vacuo and in type 1 solvents (non-HBDs Me_2SO, MeCN, Me_2CO, pyridine, and dioxane):

$$\text{rate} = k_{EXP}[1b] = 0.5 \cdot K_{CPE} \cdot k_{RC}[1b] \quad (1)$$

$$\ln\frac{k_{EXP}}{T} = -\ln 2 - \frac{\Delta G_{CPE}}{RT} - \frac{\Delta G^{\ddagger}_{RC}}{RT} + \ln\frac{RT}{h} \quad (2a)$$

$$-RT\cdot\ln\frac{k_{EXP}}{T} - RT\left(\ln 2 - \ln\frac{RT}{h}\right) = \Delta G_{CPE} + \Delta G^{\ddagger}_{RC} = \Delta G^{\ddagger}_{EXP} = \Delta G^{\ddagger}_{OBS} \quad (2b)$$

In type 2A solvents (weak HBDs $CHCl_3$, $CHBr_3$, CH_2Cl_2, and $MeNO_2$):

$$\text{rate} = k^{x}_{EXP}[1b] = 0.5 \cdot K^{x}_{SPE} K^{x}_{CPE} \cdot k^{x}_{RC}[\text{HBD}][1b] \quad (3)$$

$$\ln\frac{k^{x}_{EXP}}{T} = -\ln 2 - \frac{\Delta G^{x}_{SPE}}{RT} - \frac{\Delta G^{x}_{CPE}}{RT} - \frac{\Delta G^{x\ddagger}_{RC}}{RT} + \ln\frac{RT}{h} + \ln[\text{HBD}] \quad (4a)$$

$$-RT\cdot\ln\frac{k^{x}_{EXP}}{T} - RT\left(\ln 2 - \ln\frac{RT}{h} - \ln[\text{HBD}]\right) = \Delta G^{x}_{SPE} + \Delta G^{x}_{CPE} + \Delta G^{x\ddagger}_{RC} = \Delta G^{x\ddagger}_{EXP} = \Delta G^{\ddagger}_{OBS} + \Delta G^{x}_{SPE} \quad (4b)$$

In type 2B solvents (strong HBDs MeOH, EtOH, *i*-PrOH, *t*-BuOH, H_2O, CF_3CH_2OH, $(CF_3)_2CHOH$):

$$\text{rate} = k^*_{EXP}[1b] = 0.5 \cdot K^*_{SPE} K^*_{CPE} \cdot k^*_{RC}[ROH]^2[1b] \quad (5)$$

$$\ln\frac{k^*_{EXP}}{T} = -\ln 2 - \frac{\Delta G^*_{SPE}}{RT} - \frac{\Delta G^*_{CPE}}{RT} - \frac{\Delta G^{*\ddagger}_{RC}}{RT} + \ln\frac{RT}{h} + 2\ln[ROH] \quad (6a)$$

$$-RT\cdot\ln\frac{k^*_{EXP}}{T} - RT\left(\ln 2 - \ln\frac{RT}{h} - 2\ln[ROH]\right) = \Delta G^*_{SPE} + \Delta G^*_{CPE} + \Delta G^{*\ddagger}_{RC} = \Delta G^{*\ddagger}_{EXP} = \Delta G^{\ddagger}_{OBS} + \Delta G^*_{SPE} \quad (6b)$$

where k_{EXP}, k^x_{EXP}, and k^*_{EXP} represent the experimentally determined reaction rate for type 1, type 2A, and 2B solvents, respectively; RDH stands for the symbols of C1−C4 alcohols. In theory, a fourth possible solvation model may also exist, where three solvation molecules coordinate the oxygen of **1**, because of the presence of three nonbonding electron pairs (eqs 7 and 8):

$$\text{rate} = k^{**}_{EXP}[1b] = 0.5 \cdot K^{**}_{SPE} K^{**}_{CPE} \cdot k^{**}_{RC}[ROH]^3[1b] \quad (7)$$

$$\ln\frac{k^{**}_{EXP}}{T} = -\ln 2 - \frac{\Delta G^{**}_{SPE}}{RT} - \frac{\Delta G^{**}_{CPE}}{RT} - \frac{\Delta G^{**\ddagger}_{RC}}{RT} + \ln\frac{RT}{h} + 3\ln[ROH] \quad (8a)$$

$$-RT\cdot\ln\frac{k^{**}_{EXP}}{T} - RT\left(\ln 2 - \ln\frac{RT}{h} - 3\ln[ROH]\right) = \Delta G^{**}_{SPE} + \Delta G^{**}_{CPE} + \Delta G^{**\ddagger}_{RC} = \Delta G^{**\ddagger}_{EXP} = \Delta G^{\ddagger}_{OBS} + \Delta G^{**}_{SPE} \quad (8b)$$

It may be seen that all experimental activation parameters contain the CPE contribution (ΔG_{CPE}), where multiplication by 0.5 indicates that the formation of a pair of degenerate gauche conformers is twice as fast as that of a single anti conformer. In HBD (types 2A and 2B) solvents, the $\Delta G^{\ddagger}_{EXP}$ contains the solvent-solute pre-equilibrium (SPE) contribution (ΔG_{SPE}), originating from the complexing properties of the solvent molecules. Since we are dealing with solutions, we can only obtain the observable activation free energy ($\Delta G^{\ddagger}_{OBS}$) instead of the experimental one ($\Delta G^{\ddagger}_{EXP}$) relating to the unsolvated/uncomplexed form.

Solvents and additives (EPAs) may have two different functions. They influence the rate of the reaction by differently stabilizing the starting structure (**1c**/**1d**, **1c^x**/**1d^x**, and **1c***/**1d***) and the TS (**2**, **2^x**, and **2***), and they may stabilize the intermediate (**5**, **5^x**, and **5***) through protonation (**5** → **6**) or, in the case of EPAs, through addition to C(9) of **5^x**. It appears that strong HBD (type 2B) solvents such as ROH have dual functions: by forming hydrogen bonds with the oxygen of *N*-oxide **1** (Scheme 2), they reduce the nucleophilicity of the negatively charged oxygen atom, and they are also involved in the C(9) protonation of the ring-closed isoxazolidine intermediate (**5*** → **6***). Weak HBD (type 2A) and EPA molecules have only one function: they reduce the nucleophilicity of the oxygen. Non-HBD (type 1) solvents influence the process only via their relative permittivities (ϵ_{rel}).

2. Methods

2.1. Experimental Methods. By means of kinetic measurements, we examined the rate-determining first step of transformation of *N*-oxide **1** in a number of solvents, and the rates of the reactions were measured at different temperatures. Since traces of water may lead to false-positive data, the cooled solutions of **1** were dried with molecule sieve (Aldrich, 4 Å, 5 μm, without extra activation), and the residual water content (∼0.2%) was checked by NMR. ^{1}H NMR spectroscopy was used for non-HBD solvents (Me_2SO, MeCN, $PhNO_2$, Me_2CO, pyridine, *t*-BuOH, and dioxane) and for weak HBD solvents ($MeNO_2$, CH_2Cl_2, $CHCl_3$, and $CHBr_3$). The NMR methods used, together with characteristic chemical shifts, are listed in Table S1 in the Supporting Information. GC measurements were applied for strong HBD solvents (H_2O, MeOH, EtOH, CF_3CH_2OH, *i*-PrOH, $(CF_3)_2CHOH$, and *t*-BuOH). The experimental conditions of GC measurements were the same as described in ref 16. For the solvents MeCN, H_2O, MeOH, EtOH, *i*-PrOH, *t*-BuOH, CH_2Cl_2, and $CHCl_3$, the Gibbs free energy ($\Delta G^{\ddagger}_{OBS}$), enthalpy ($\Delta H^{\ddagger}_{OBS}$), and entropy ($\Delta S^{\ddagger}_{OBS}$) of activation were calculated from the reaction constants determined at various temperatures. The $\Delta G^{\ddagger}_{OBS}$ and $\Delta H^{\ddagger}_{OBS}$ values in other solvents were obtained through comparison of the rate constants with those determined in MeCN. To calculate $\Delta G^{\ddagger}$, $\Delta H^{\ddagger}$, and $\Delta S^{\ddagger}$ values, the Eyring equation was used.[16,41] Rate constants and activation parameters obtained for the transformation of **1** in MeOH, EtOH, and *i*-PrOH were published earlier.[16] Parameters for other solvents are reported in this article (see Table 3).

2.2. Computational Methods. 2.2.1. Ab Initio Methods and Basis Set Error (BSE). The geometries and vibrational frequencies were calculated by using the Gaussian03[1−4,42] program in vacuo and in solvents, using the default PCM method (integral equation formalism polarizable continuum medium, IEF-PCM, or PCM in brief) at the same B3LYP/6-31++G(d,p)[43] theoretical level. The effects of the applied computational method (HF, B3LYP, MP2(fc),[44] and MP4(fc)[45]) and basis set were also examined (Table S2 in the Supporting Information). The difference between the energy values obtained at the B3LYP/6-311++G(2d,2p) and B3LYP/6-31++G(d,p) levels of theory was 1.95 kJ mol^{-1}, and we used this value ($\Delta E^{\ddagger}_{BSE}$) to correct for BSE. Because of convergence problems, in the case of the explicit−implicit solvent model, the geometry optimization was halted when, after at least 50−100 optimization steps, the energy differences within the last five optimization steps were below 0.3 kJ mol^{-1}.

2.2.2. Entropy Calculations. The entropy contribution of the hindered rotation of the propargyl group in *N*-oxide **1** was taken into account by using the free rotation entropy formula (eq 9) instead of the vibration entropy (eq 10).[46−48] The $I = h^2/8\pi^2\Theta k_B$; ($\Theta = hc\omega/k_B$) value, where Θ is the characteristic rotational temperature, h is the Planck constant, k_B is the Boltzmann constant, c is the speed of light, and ω is the torsional vibration of the propargyl group ($\omega = 87.4\ \text{cm}^{-1} = 8740\ \text{m}^{-1}$), which was obtained from frequency calculations. The variable σ_{int} is the rotational symmetry number ($\sigma_{int} = 1$).

$$S_{free.rot} = R\left\{\ln\left[\frac{(8\pi^3 I_{int} k_B T)^{1/2}}{\sigma_{int} h}\right] + \frac{1}{2}\right\} = R\ln\left(\frac{\pi T}{\sigma^2_{int}\Theta}\right)^{1/2} + \frac{1}{2}R = R\ln\left(\frac{\pi k_B T}{\sigma^2_{int} c\omega_i h}\right)^{1/2} + \frac{1}{2}R = R\ln\left[\frac{\pi k_B (313\ \text{K})}{ch(8740\ \text{m}^{-1})}\right]^{1/2} + \frac{1}{2}R = 16.30\ \text{J mol}^{-1}\ \text{K}^{-1} \quad (9)$$

(38) Alkorta, I.; Elguero, J. *J. Phys. Chem. A* **1999**, *103*, 272−279.
(39) Abboud, J.-L. M.; Sraidi, K.; Abraham, M. H.; Taft, R. W. *J. Org. Chem.* **1990**, *55*, 2230−2233.
(40) Frange, B.; Abboud, J.-L. M.; Benamou, C.; Bellon, L. *J. Org. Chem.* **1982**, *47*, 4554−4557.
(41) Ruff, F.; Csizmadia, I. G. *Organic Reactions: Equilibria, Kinetics and Mechanism*; Elsevier: Amsterdam, 1994; Chapter 6, p 141.
(42) Frisch, M. J. et al. *Gaussian 03*, Revision 6.0; Gaussian, Inc.: Pittsburgh, PA, 2003.
(43) Beke, A. D. *J. Chem. Phys.* **1993**, *98*, 5648−5651.
(44) Head-Gordon, M.; Pople, J. A.; Frisch, M. J. *Chem. Phys. Lett.* **1988**, *153*, 503−506.
(45) Krishnan, R.; Pople, J. A. *Int. J. Quantum Chem.* **1978**, *14*, 91−100.
(46) Cramer, C. J. *Essentials of Computational Chemistry*; Wiley & Sons: West Sussex, England, 2001; Chapter 10, pp 319−344.
(47) Pitzer, K. S.; Gwinn, W. D. *J. Chem. Phys.* **1942**, *10*, 428−440.
(48) Forst, W. *Theory of Unimolecular Reactions*; Academic Press: New York, 1973; Chapter 11, p 366.

$$S_{\text{vib}} = R\frac{hc\omega_i}{k_B T[\exp(hc\omega_i/k_B T) - 1]} - R\ln[1 - \exp(hc\omega_i/k_B T)] = R\frac{hc(8740\ \text{m}^{-1})}{k_B T\{\exp[hc(8740\ \text{m}^{-1})/k_B(313\ \text{K})] - 1\}} - R\ln\{1 - \exp[hc(8740\ \text{m}^{-1})/k_B(313\ \text{K})]\} = 9.19\ \text{J mol}^{-1}\ \text{K}^{-1} \quad (10)$$

When the other frequencies were left fixed, the final corrected entropy value of the ring-closure step was $\Delta S^{\ddagger}_{\text{CORR}} = -14.24$ J mol^{-1} K^{-1} in vacuo, which is near the observed experimental value. This entropy value was used in the description of the ring-closure step.

2.2.3. Molecular Dynamic (MD) Simulations. The MD simulation of the first solvation shell was carried out by using the Hyperchem 7.0 program[49] with 256 equilibrated solvent molecules in a box under periodic boundary conditions and correct dimensions (20−33 Å); the shifted cutoffs[49] were 12.5 and 16.5 Å. The Amber 99 force field[50] method was used, lasting for 300 ps − 1 ns after 20 ps of the equilibrium process. For charge parametrizations of the **1a**, **1b**/**1c**, **2**, H_2O, MeOH, EtOH, *i*-PrOH, *t*-BuOH, CH_4, CH_2Cl_2, and $CHCl_3$ molecules in MD simulations, the B3LYP/6-31++G(d,p) level of theory and natural bond orbital (NBO) version 3 analysis[51] were applied (Table S3 in the Supporting Information).

The radial distribution function (RDF)[52] of the OH or CH proton and that of the oxygen in *N*-oxide **1** and TS **2** for different solvents was calculated by using eq 11:

$$\text{RDF}(r) = \frac{\langle\sum_{i=1}^{N}\delta[r - r_{\text{O}-\text{H}_i}]\rangle \cdot V}{4\pi r^2 \cdot \Delta r \cdot N} \quad (11)$$

where N is the total number of OH or CH protons within the volume element, δ is the Dirac delta function, $r_{\text{O}-\text{H}_i}$ is the radial distance of the *N*-oxygen from the OH or CH of the solvent molecule, V is the volume of the simulated box, and $4\pi r^2\Delta r$ is the spherical shell.

3. Results

3.1. Hydrogen Bonding of N−O Functionality. As indicated in Section 1.3, in HBD solvents three different solvations models can be set up for which quite diverse kinetic and activation parameters are assumed. Expectations were confirmed by preliminary DFT [B3LYP/6-31++G(d,p)] calculations. For the models with one, two, and three explicit solvating MeOH molecules in vacuo, the computed $\Delta E^{\ddagger}$ values referring to the rate-determining ring-closure (RC) step were 86.2,[17] 101.5,[17] and 120.1 kJ mol^{-1}, respectively. The different values clearly indicate that the creation of a suitable chemical model with the correct number of solvating molecules (solvation number, SN) is essential for DFT calculations. This correct SN in various solvents was determined by using theoretical MD simulations.

3.1.1. Experimental Observations Indicative of Hydrogen Bonding (HB). Experimental evidence of existing HB may provide a good tool to reinforce our theoretical results.

Solubility. The simplest way to estimate the solvent effects is to investigate the solubilities of a given compound in different solvents. The solubility of the *N*-oxide **1** was found to be relatively high in solvents where the rearrangement proceeds slowly, whereas it proved poor in solvents that increase the rate of the rearrangement. For solubility data, see the Supporting Information. The solubility of **1** increased significantly when minimal amounts of water or EPA were added, pointing to the complexation effects exerted by HBD solvents and EPAs.

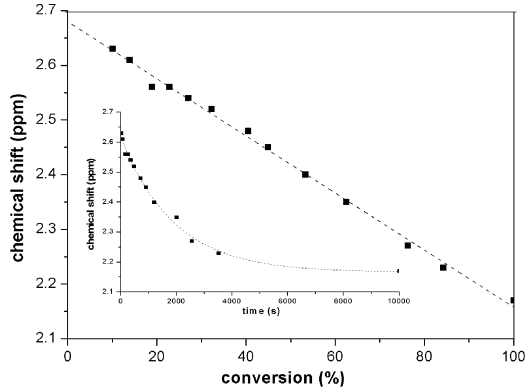

Figure 1. Shift of the water proton signal during the Meisenheimer transformation of *N*-oxide **1** in MeCN containing 2 equiv of water.

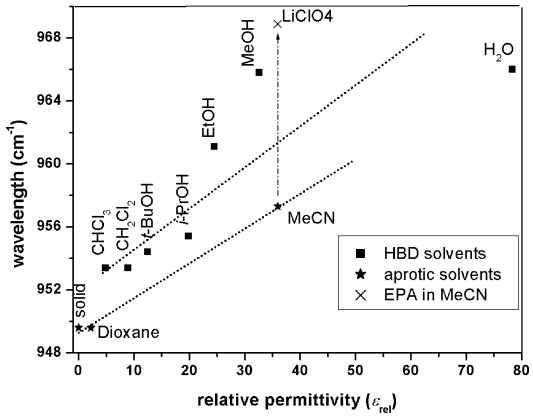

Figure 2. The ν(NO) frequency of *N*-propargylmorpholine *N*-oxide (**1**) in different solvents and in MeCN solutions containing $LiClO_4$. The arrow indicates the shift in the IR band in MeCN after the addition of $LiClO_4$.

NMR Spectroscopy. Convincing evidence of HB was furnished by NMR. When the rearrangement of *N*-oxide **1** in MeCN or CH_2Cl_2 in the presence of 2 equiv of water or MeOH was followed by NMR, the chemical shift of the OH proton moved toward lower values as the reaction proceeded (i.e., the concentration of **1** decreased; Figure 1).

At the end of the reaction, the chemical shift of the water proton reached the normal value of 2.15 ppm, because product **3** is much less capable of forming HB.

IR Spectroscopy. *N*-Oxide **1** in the solid state exhibits an IR band at ∼950 cm^{-1}, assigned to the vibrational frequency of the N−O group. This band is assumed to exhibit characteristic shifts in solution, depending on the relative permittivity and the HBD and EPA ability of the solvents. Figure 2 shows the shifts of the ν(NO) band in non-HBD (dioxane and MeCN) and HBD (H_2O, MeOH, EtOH, *i*-PrOH, *t*-BuOH, CH_2Cl_2, and $CHCl_3$) solvents and in MeCN solutions containing an EPA additive ($LiClO_4$). It may be seen that the ν(NO) band appears at significantly higher frequencies in strong HBD solvents than in non-HBD media, due to the existence of HB of different strengths between the solute and solvent molecules. An ex-

(49) *Hyperchem*, version 7.04; Hyperchem Inc.: Gainesville, FL, 2003.
(50) Cornell, W. D.; Cieplak, P.; Bayly, C. I.; Gould, I. R.; Merz, K. M.; Ferguson, D. M.; Spellmeyer, D. C.; Fox, T.; Caldwell, J. W.; Kollman, P. A. *J. Am. Chem. Soc.* **1995**, *117*, 5179−5197.
(51) Carpenter, J. E.; Weinhold, F. *J. Mol. Struct. (THEOCHEM)* **1988**, *169*, 41−62.
(52) Cramer, C. J. *Essentials of Computational Chemistry*; Wiley & Sons: West Sussex, England, 2001; Chapter 3, pp 63−94.

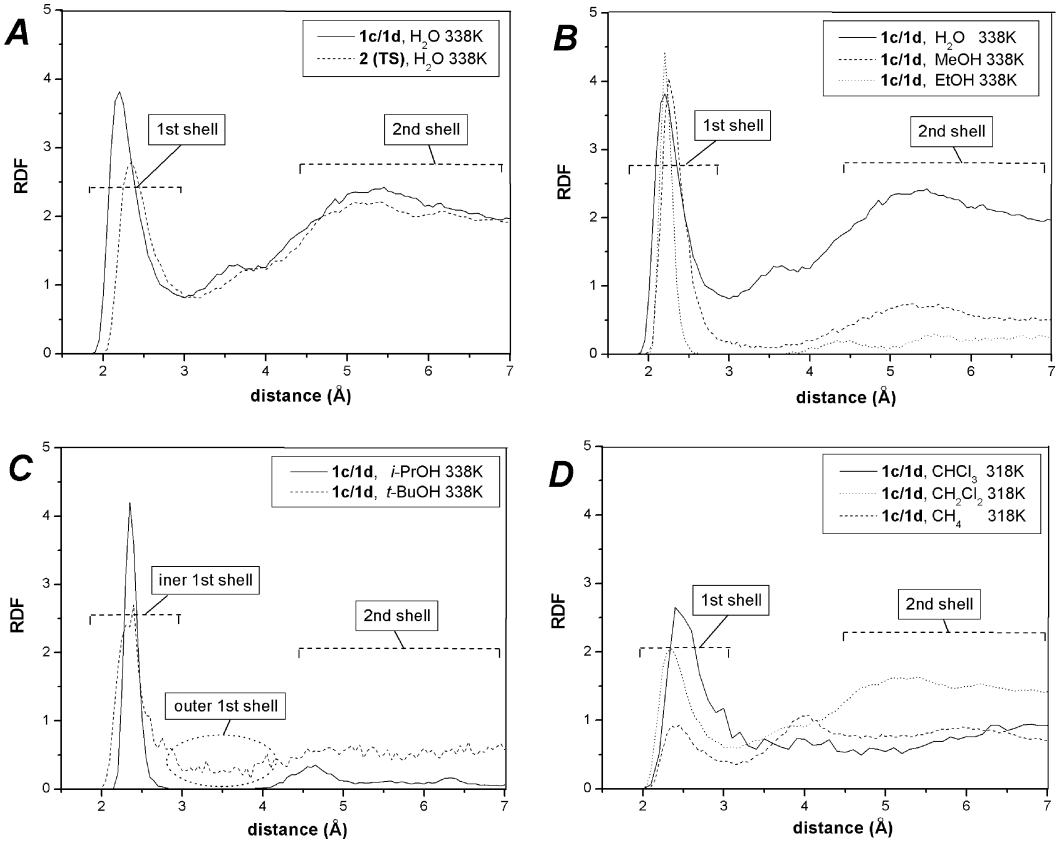

Figure 3. RDF for different solvents. (A) H_2O. (B) H_2O, MeOH, and EtOH. (C) *i*-PrOH and *t*-BuOH. (D) $CHCl_3$, CH_2Cl_2, and CH_4.

Table 1. Results of MD Studies on Different Conformers of *N*-Propargylmorpholine *N*-Oxide (**1b**, **1c**/**1d**) and the TS (**2**) in Various Solvents (SN = Solvation Number)

	1b			1c/1d			2			
	integral[a] SN	max (Å)[b]	width (Å)[c]	integral[a] SN	max (Å)[b]	width (Å)[c]	integral[a] SN	max (Å)[b]	width (Å)[c]	exchange (ps)[d]
H_2O	2.50	2.10	~0.80	2.44	2.10	~0.80	2.14	2.35	~0.95	~100
MeOH	2.40	2.25	~0.90	2.34	2.20	~0.90	2.05	2.35	~1.05	~200
EtOH	2.11	2.20	~0.75	2.15	2.20	~0.90	1.95	2.35	~0.95	~200
i-PrOH	2.09	2.40	~1.00	2.01	2.40	~1.00	1.91	2.40	~1.00	~300
t-BuOH	1.22[e]	2.45	~1.10	1.20[e]	2.40	~1.10	1.24[e]	2.45	~1.10	>300
CH_2Cl_2	1.10	2.50	~1.00	1.02	2.50	~1.00	1.05	2.40	~1.10	~80
$CHCl_3$	1.79	2.40	~1.10	1.67	2.40	~1.10	1.25	2.35	~1.10	~100
CH_4	1.15	2.50	~1.20	1.10	2.50	~1.20	0.85	2.50	~1.20	~35

[a] Integral value for the first solvating shell (1.9−~3.0 Å). [b] Maximum extent of the first solvating shell. [c] Approximate width of the first solvating shell. [d] Approximate exchange rate of the solvating molecules in the first solvating shell. [e] Only for the first solvating shell.

tremely high shift occurs when a complex is formed between Li^+ ions and *N*-oxide molecules.

3.1.2. Molecular Dynamics Simulations. To answer the question of how many solvent molecules are required for accurate modeling of the Meisenheimer rearrangement of *N*-oxide **1**, MD simulations were performed. Since the activation energy depends on the structure of both the starting structure and the TS, the solvation of TS structures in different solvents was also studied. To determine the XH-hydrogen−*N*-oxygen RDF (eq 11, Figure 3) of the starting structures **1b**, **1c**/**1d**, and **2** in different solvents, calculations were carried out for strong HBD solvents (H_2O, MeOH, EtOH, *i*-PrOH, and *t*-BuOH), and weak HBD solvents ($CHCl_3$ and CH_2Cl_2) at reaction temperatures of 338 and 313 K. To study the RDFs of non-HBD solvents, liquid methane (high pressure) was applied (Figure 3).

The shape of the RDF in different strong HBD solvents is similar, containing a high, narrow peak that relates to the first solvating shell and a smaller, broad peak relating to the second solvating shell. The average $O-H\cdots{}^{-}O-N^{+}$ distance for all the studied solvents was about 2.0−2.45 Å (Table 1). The narrowest functions were obtained for water and MeOH, whereas *t*-BuOH exhibited a much broader distribution. In all strong HBD media except *t*-BuOH, roughly two OH groups participated in a coordinative HB to the *N*-oxygen of **1b** and **1c**/**1d**.

In the case of *t*-BuOH, two first solvating shells exist at different distances. The SN of the nearer one (2.45 Å) is 1.2, while the farther one (3.2−5 Å) contains an additional 0.8 OH, revealed as a small broad shoulder. This means that *t*-BuOH has a specific solvating shell, probably due to the bulkiness of its molecules (see also Section 3.2.2). Thus, *t*-BuOH represents a special class of HBD solvents. The split of the first solvating shell indicates that *t*-BuOH requires a more complex approach. The significantly smaller $\Delta G^{\ddagger}$ in *t*-BuOH as compared with that in *i*-PrOH may be explained by a sophisticated complexing

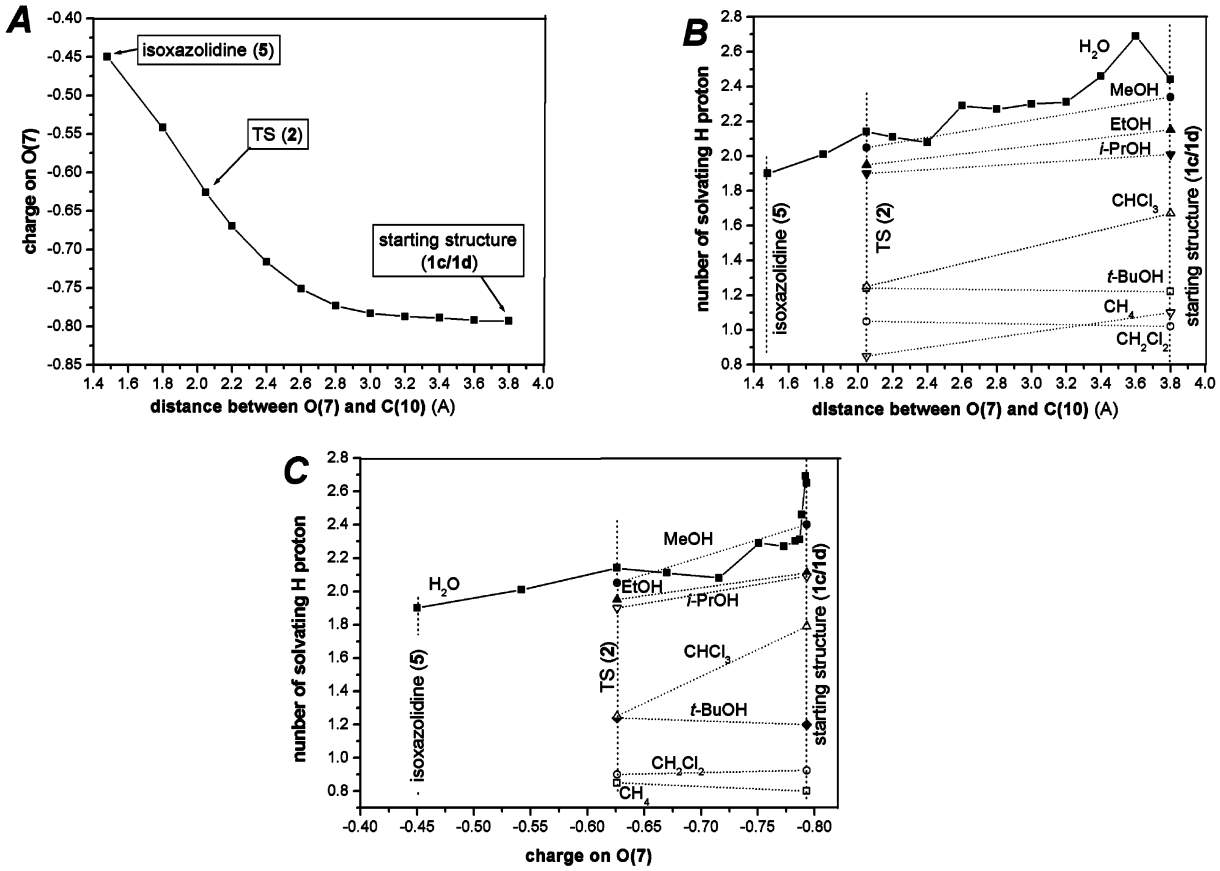

Figure 4. (A) Change in the NBO charge of O(7) during the reaction (**1c**/**1d** → **2**). (B) The number of solvent molecules (SN) in the first solvating shell, obtained from the RDFs for **1c**/**1d** and **2**. (C) The number of solvent molecules (SN) in the first solvating shell when O(7) has a different charge.

equilibrium process between *t*-BuOH and the *N*-oxide (**1b** and **1c**/**1d**).

Surprisingly, $CHCl_3$ displays a relatively high SN (1.6 molecules of solvent/solute), but this is still significantly smaller than those of strong HBD solvents. CH_2Cl_2 gives a very small first solvating shell, composed of about 1.2 equiv of solvent molecules. The peak of RDF proved to be very wide (2.2−3.5 Å), revealing a weak and unsure HB effect. The methane solution chosen as non-HBD solvent reference gave a very broad and uncertain first peak (2.2−3.6 Å), with roughly only one hydrogen atom in the first solvating shell, at an appreciable distance (2.5 Å) from O(7).

The DFT calculation [B3LYP/6-31++G(d,p)] shows that the charge of O(7) decreases from the starting gauche structure **1c**/**1d** to TS **2**, which may be associated with a difference in solvation of **1c**/**1d** and TS **2**. To examine the change in the SN of the water molecules around the *N*-oxygen during the reaction, 12 MD simulations (50 ps) were carried out in water with decreasing C(10)−O(7) distances (3.8−1.6 Å), mimicking the reaction coordinates from the starting gauche structure **1c**/**1d** to isoxazolidine **5** through TS **2** (Figure 4), with continuous change of the charges (see the protocol in Section 2.2). The number of solvating H_2O molecules significantly decreases toward TS **2** and **5**. However, there are two reasons for this decrease: the first is the decreasing charge of O(7) (Figure 4), and the second is the increasing steric hindrance of the approaching propargyl group.

In the case of the TS structure (**2**), the SN values of XH (X = C or O) are significantly smaller than those of the starting structures **1b** and **1c**/**1d**. With the exception of *t*-BuOH, roughly two HBD protic solvent molecules play important roles in the solvation, whereas in the case of *t*-BuOH only one molecule belongs closely to the first solvating shell. In summary, two strong HBD solvent molecules must be considered in the primary solvation shell model for direct solvation studies involving DFT calculations.

For weak HBD, halogenated solvents, the TS structure (**2**) is complexed with roughly 1 equiv of solvent molecules, indicating that exact consideration for only one solvent molecule is sufficient for the DFT calculations.

The exchange of the solvent molecules around the *N*-oxygen proved to be very fast (∼10−100 ps). Accordingly, the separate sign of the OH proton in the solvating molecule cannot be observed in low-temperature NMR experiments since the time scale is set in milliseconds.

3.1.3. DFT Study of HB. The strengths of HB (complexation energies, ΔE_1 and ΔE_2) between *N*-oxide **1** and different HBD molecules were determined by theoretical methods, ignoring the basis set superposition error (BSSE), which proved to be marginally different, as shown in preliminary calculations. We calculated ΔE_1 and ΔE_2 via eqs 12 and 13, respectively:

$$\Delta E_1 = E_{\text{complex}}1 - (E_{\text{HBD/EPA}} + E_{N-\text{oxide}}) \qquad (12)$$

$$\Delta E_2 = E_{\text{complex}}2 - (2E_{\text{HBD/EPA}} + E_{N-\text{oxide}}) \qquad (13)$$

All molecules were optimized in vacuo and with the PCM method, using the appropriate relative permittivity (Table 2). As shown in Table 2, the values obtained for the explicit solvent

Table 2. Calculated Energies (kJ mol^{-1})[a] and O(7)···X[b] Distances (Å)[a] Obtained by Different Computational Methods for Complexes Formed between *N*-Propargylmorpholine *N*-Oxide (**1**) and Strong HBDs, Weak HBDs, and EPAs

	explicit method					explicit–implicit method				
	ΔE_1	d_1	ΔE_2	d_2	$\Delta E_2 - \Delta E_1$	ΔE_1	d_1	ΔE_2	d_2	$\Delta E_2 - \Delta E_1$
H_2O	−68.12		−126.80	1.77	−58.67	−8.39	1.71	−8.72	1.75	−0.33
H_2O[c]						−8.14	1.71	−8.48	1.76	−0.34
MeOH	−42.56	1.71	−76.05	1.78	−33.49	−9.16	1.70	−11.38	1.75	−2.22
EtOH	−41.92	1.73	−73.45	1.79	−31.54	−7.64	1.71	−6.57	1.77	1.07
CF_3CH_2OH	−62.77	1.61	−109.04	1.69	−46.24	−5.28	1.59	−26.75	1.70	−21.46
i-PrOH	−42.03	1.76	−70.59	1.82	−28.57	−3.39	1.76	0.67	1.78	4.07
$(CF_3)_2CHOH$	−64.16	1.54	−113.58	1.65	−49.43	−10.16	1.56	−14.88	1.64	−4.72
t-BuOH	−39.33	1.76	−68.05	1.83	−28.71	−3.36	1.77	2.73	1.84	6.08
CH_2Cl_2	−24.91	2.02	−44.07	2.06	−19.16	−3.49	2.05	−8.59	2.03	−5.10
$CHCl_3$	−30.40	1.93	−53.45	1.99	−23.05	−10.17	1.91	−18.78	2.00	−8.61
$MeNO_2$	−31.37	2.05				−3.36[c]	2.07[c]			
CH_4	−0.71	2.53				3.70[c]	6.50[c]			
H^+	−966.74	1.06				−1157.61[c]	1.09[c]			
Li^+	−284.17	1.76				−4.19[c]	1.84[c]			
Na^+	−208.23	2.12				−5.48[c]	2.22[c]			
BF_3	−115.15	1.56				−124.87[c]	1.51[c]			
BF_3:OEt_2	−79.03	1.56				−70.74[c]	1.51[c]			

[a] Subscripts 1 and 2 relate to complexation with one or two HBD and EPA molecules. [b] X = H for solvents (and acids) or alkaline ions or boron atom. [c] Obtained with MeCN solvent model.

model (in vacuo) differ significantly from the results obtained with the implicit−explicit model, and the former does not appear to be realistic. Thus, only the energies obtained with the PCM method will be discussed. As expected, $(CF_3)_2CHOH$, CF_3CH_2OH, and water undergo the strongest HB, the HB strength decreasing significantly toward *t*-BuOH. Increase of the number of chlorine atoms in the solvent molecule (from CH_4 to $CHCl_3$) significantly increases the complexation energies. Surprisingly, the HB strength of $CHCl_3$ proved to be very high and was similar to those of strong HBD solvents. Large differences can be observed if one or two solvating molecules take part in the solvation in different strong HBD solvents, indicating that the second solvation is higher in energy. This energy has a + sign for EtOH (1.07 kJ mol^{-1}), *i*-PrOH (4.07 kJ mol^{-1}), and *t*-BuOH (6.08 kJ mol^{-1}). In the cases of H_2O, MeOH, and EtOH, the complexation energies [$\Delta E_3 = E_{\text{complex}}3 - (3E_{\text{HBD}} + E_{\text{N-oxide}})$] of the solvation by the third solvent molecule were higher than ΔE_2. [$\Delta E_3(H_2O) - \Delta E_2(H_2O) = 1.18$ kJ mol^{-1}; $\Delta E_3(\text{MeOH}) - \Delta E_2(\text{MeOH}) = 2.78$ kJ mol^{-1}; $\Delta E_3(\text{EtOH}) - \Delta E_3(\text{EtOH}) = 4.30$ kJ mol^{-1}.] These values suggest that unfavorable complexation effects may occur if a third solvating molecule is considered. The energy values also indicate that the first solvating shell with two solvent molecules is preferred with H_2O, MeOH, EtOH, and *i*-PrOH as solvents ($\Delta E_2 = -8.72$, −11.38, −6.57, and +0.67 kJ mol^{-1}, respectively), but in *t*-BuOH the effect of the second molecule is less significant (Table 2).

EPAs also have very significant complexation energies (Table 2). H^+ and BF_3 (corrected for the effect of diethyl ether, $\Delta E_1 = E_{N-\text{oxide}-BF3} + E_{OEt2} - (E_{BF3:OEt2} + \Delta E_{N-\text{oxide}-BF3})$ possess the largest complexation energies, while Li^+ and Na^+ too have significant effects.[53]

3.2. Experimental Kinetics. 3.2.1. Kinetic Studies in Non-HBD (Aprotic) Solvents. Activation parameters ($\Delta H^{\ddagger}_{\text{OBS}}$, $\Delta G^{\ddagger}_{\text{OBS}}$, and $\Delta S^{\ddagger}$) calculated from the unimolecular rate constants (k), obtained under standard conditions (see Section 2) at given temperatures for the first step of the rearrangement of *N*-oxide **1** in various aprotic solvents, are shown in Table 3. Relative reaction constants at 313 K (k_{rel}) are also shown, as compared with the standard k_{rel} value of 1, referring to water-free MeCN solution at 313 K ($\Delta H^{\ddagger}_{\text{OBS}} = 94.7$ kJ mol^{-1}, $\Delta G^{\ddagger}_{\text{OBS}} = 89.0$ kJ mol^{-1}, $\Delta S^{\ddagger} = -17.1$ J mol^{-1} K^{-1}). Solvents are listed in the sequence of decreasing relative permittivities (ϵ_{rel}).[54,55] In Figure 5, $\Delta G^{\ddagger}_{\text{OBS}}$ values are plotted against the relative permittivity of the solvents.

In dry non-HBD media (type 1), the k_{rel} and $\Delta G^{\ddagger}_{\text{OBS}}$ values lie in the ranges 0.67−2.27 and 92.7−95.9 kJ mol^{-1}, respectively, demonstrating fast reactions as compared with those in other types of solvents. The Kirkwood−Onsager rules[23,56] predict a linear increase in $\Delta G^{\ddagger}_{\text{OBS}}$ according to $1/\epsilon_{\text{rel}}$ for ionic molecules and $2(\epsilon_{\text{rel}} - 1)/(2\epsilon_{\text{rel}} - 1)$ for dipolar molecules, and our experimentally obtained data for non-HBD solvents fit in with this rule. As a consequence of its larger dipole moment, the starting structure **1c**/**1d** is better solvated than TS **2**, which results in a slight increase in $\Delta G^{\ddagger}_{\text{OBS}}$ as the ϵ_{rel} or $2(\epsilon_{\text{rel}} - 1)/(2\epsilon_{\text{rel}} - 1)$ value of the solvent increases.

In the absence of an exchangeable proton, in a non-HBD (aprotic) solvent, only the Meisenheimer rearrangement takes place and the product progressively decomposes to other derivatives.[16]

3.2.2. Weak and Strong HBD Solvents. In contrast with the non-HBD (aprotic) solvents, the reaction rates were significantly lower in HBD (protic) media, reflecting the larger $\Delta G^{\ddagger}_{\text{OBS}}$. In type 2A solvents (e.g., in dry $CHBr_3$, $CHCl_3$, CH_2Cl_2, and $MeNO_2$), the k_{rel} and $\Delta G^{\ddagger}_{\text{OBS}}$ values (0.67−0.22 and 96.0−98.8 kJ mol^{-1}, respectively) fall between those observed for type 1 and 2B solvents, suggesting a weak HBD effect. It should be mentioned that CH_2Cl_2 and $MeNO_2$, with $k_{\text{rel}} = 0.67$ and 0.52 and $\Delta G^{\ddagger}_{\text{OBS}} = 96.0$ and 96.6 kJ mol^{-1}, respectively, exhibit a very weak HBD effect. In strong HBD solvents of type 2B, the reactions proceed much more slowly: $k_{\text{rel}} = 0.032-1.98 \times 10^{-3}$, $\Delta G^{\ddagger}_{\text{OBS}} = 104.6-111.0$ kJ mol^{-1}, $\Delta H^{\ddagger}_{\text{OBS}} = 97.6-107.3$ kJ mol^{-1}, $\Delta S^{\ddagger} = (-9.6) - (-20.6)$ J mol^{-1} K^{-1}.

(53) Maria, P.-C.; Gal, J.-F. *J. Phys. Chem.* **1985**, *89*, 1296−1304.
(54) Abboud, J.-L. M.; Notario, R. *Pure Appl. Chem.* **1999**, *71*, 645−718.
(55) Evans, E.; McElroy, A. *J. Solution Chem.* **1975**, *4*, 413−430.
(56) Kirkwood, J. G. *J. Chem. Phys.* **1934**, *2*, 351−361.

Table 3. Rate Constants and Activation Parameters ($\Delta G^{\ddagger}_{OBS}$) Obtained for the First Step of the Rearrangement of *N*-Propargylmorpholine *N*-Oxide (**1**) in Different Solvents (for Experimental Conditions, See the Supporting Information)

solvent	ϵ_{rel}[a]	T (K)	k (s^{-1})	k^{o} (s^{-1})[b]	k_{rel}	$\Delta H^{\ddagger}_{OBS}$ (kJ mol^{-1})[c]	$\Delta G^{\ddagger}_{OBS}$ (kJ mol^{-1})	$\Delta S^{\ddagger}$ (J mol^{-1} K^{-1})
D_2O	80.00	338	5.03×10^{-5}	2.41×10^{-6}	2.80×10^{-3}	106.6	110.1	−9.6
H_2O[d]	78.36	338	3.92×10^{-5}	1.70×10^{-6}	1.98×10^{-3}	107.3	111.0	−9.6[e]
Me_2SO[f]	46.70	313	6.50×10^{-4}	6.50×10^{-4}	0.67	90.0	95.9	−17.1[g]
$MeNO_2$[f]	38.22	313	4.51×10^{-4}	4.51×10^{-4}	0.52	90.7	96.6	−17.1[g]
MeCN[f,h]	**35.94**	**313**	$\mathbf{8.61 \times 10^{-4}}$	$\mathbf{8.61 \times 10^{-4}}$	**1.00**	**89.0**	**94.8**	**−17.1**
$PhNO_2$[f]	34.78[j]	313	1.31×10^{-3}	1.31×10^{-3}	1.52	87.9	93.8	−17.1[g]
MeOH[i]	32.66	338	6.04×10^{-5}	2.81×10^{-6}	3.26×10^{-3}	105.0	109.7	−17.1[g]
CF_3CH_2OH	26.53[j]	338	5.00×10^{-5}	1.98×10^{-6}	2.30×10^{-3}	104.5	110.4	−17.1[g]
EtOH[i]	24.55	338	7.22×10^{-5}	4.29×10^{-6}	4.98×10^{-3}	103.7	108.6	−15.7
Me_2CO[f]	20.70	313	1.86×10^{-3}	1.86×10^{-3}	2.17	87.0	92.8	−17.1[g]
$(CF_3)_2CHOH$	∼20[k]	332	7.01×10^{-5}	4.75×10^{-6}	5.52×10^{-3}	104.8	110.9	−17.1[g]
i-PrOH[i]	19.92[j]	338	1.63×10^{-4}	8.59×10^{-6}	9.98×10^{-3}	101.0	106.8	−17.1[g]
pyridine[f]	12.91[j]	309	9.73×10^{-4}	1.54×10^{-3}	1.79	87.6	93.4	−17.1[g]
t-BuOH[i]	10.36[j]	338	4.70×10^{-4}	1.99×10^{-5}	0.0231	97.6	104.6	−20.6
CH_2Cl_2[f]	8.93	313	5.75×10^{-4}	5.75×10^{-4}	0.67	90.0	96.0	−17.1[g]
$CHCl_3$[f]	4.90	313	1.91×10^{-4}	1.91×10^{-4}	0.22	92.9	98.8	−17.1[g]
$CHBr_3$[f]	4.35[j]	323	6.07×10^{-4}	1.98×10^{-4}	0.23	92.3	98.2	−17.1[c]
dioxane[f]	2.21	309	1.15×10^{-2}	8.00×10^{-3}	0.11	83.1	89.0	−17.1[g]

[a] Taken from the Gaussian03 program based on IUPAC data.[54] [b] Calculated for 313 K. [c] Estimated from $\Delta G^{\ddagger}_{OBS}$, assuming that $\Delta S^{\ddagger}$ is constant (−17.1 J mol^{-1} K^{-1}) for different solvents. [d] Values corrected by taking the inverse α secondary isotope effect into account (see Section 3.2.3). [e] Estimated value equal to that obtained for D_2O. [f] Deuterated solvent. [g] Estimated value equal to that obtained for MeCN. [h] Reference solvent. [i] Taken from ref 16. [j] Taken from ref 17. [k] Taken from ref 55.

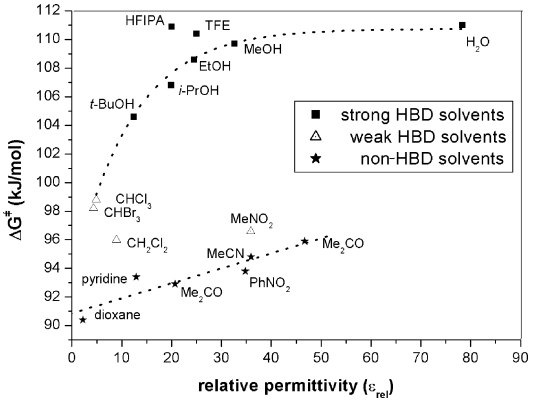

Figure 5. $\Delta G^{\ddagger}_{OBS}$ values for the first step of the rearrangement of *N*-propargylmorpholine *N*-oxide (**1**), obtained from kinetic measurements in different solvents.

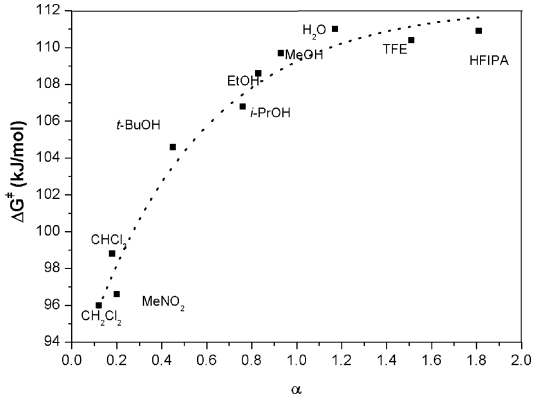

Figure 6. $\Delta G^{\ddagger}_{OBS}$ values as compared with α values,[57] proportional to the HBD ability of the given solvent. TFE = CF_3CH_2OH; HFIPA = $(CF_3)_2CHOH$.

In Figure 6, the $\Delta G^{\ddagger}_{OBS}$ values are plotted against the α values,[57−60] which are proportional with the HBD ability of the solvents. The α values were calculated by multilinear regression of the solvatochromic effect values obtained for 4-nitroaniline derivatives.

As expected, the two fluorinated solvents [CF_3CH_2OH and $(CF_3)_2CHOH$] and water are involved in the strongest HB with *N*-oxide **1**, causing slow reactions as compared with other solvents. It is interesting to compare the effects of the two fluorinated solvents with those of the related nonfluorinated ones (EtOH and *i*-PrOH); stronger HB significantly decreases the reaction rate. The position of *t*-BuOH in Figures 5 and 6 is rather special; *t*-BuOH does not closely belong to the strong HBD solvents (the series from water to *i*-PrOH), but it cannot be ranked among the weak HBD solvents ($CHCl_3$, $CHBr_3$, CH_2Cl_2, and $MeNO_2$) either. The special HB pattern of *t*-BuOH may be attributed to the bulkiness of its molecules causing steric hindrance around the *N*-oxygen.[40] From the MD studies, we concluded that the first solvating shell of *t*-BuOH is not uniform: it splits into two parts, as described in Section 3.1.4.

The dual function of strong HBD solvents results in a slow Meisenheimer reaction, allowing the competing reaction to proceed, leading to the enamino aldehyde product (**4**) which requires a protonation step **5*** → **6*** (Scheme 2). However, a significant difference in the product distribution can be recognized in the series of solvents ranging from H_2O to *t*-BuOH, as a reflection of their different protonation and deprotonation properties. The two extreme values were observed in *t*-BuOH ([**3**]/[**4**] = 0.29) and in MeOH ([**3**]/[**4**] = 1.21), with intermediate data in EtOH ([**3**]/[**4**] = 0.66) and in *i*-PrOH ([**3**]/[**4**] = 0.50).[16] Both the α and the acity[61] parameters (anion-solvating property, obtained from nonlinear regression of numerous physical and chemical properties of solvents) of the solvents display a good relationship with the observed product distribution.[16] In weak

(57) Laurence, C.; Nicolet, P.; Dalati, M. T.; Abboud, J.-L. M.; Notario, R. *J. Phys. Chem.* **1994**, *98*, 5807−5816.
(58) Kamlet, M. J.; Abboud, J.-L. M.; Abraham, M. H.; Taft, R. W. *J. Org. Chem.* **1983**, *48*, 2877−2887.
(59) Marcus, Y. *Chem. Soc. Rev.* **1993**, *22*, 409−416.
(60) Cramer, C. J. *Essentials of Computational Chemistry*; Wiley & Sons: West Sussex, England, 2001; Chapter 7, p 433.
(61) Swain, C. G.; Swain, M. S.; Powell, A. L.; Alunni, S. *J. Am. Chem. Soc.* **1983**, *105*, 502−513.

HBD solvents ($CHCl_3$, $CHBr_3$, CH_2Cl_2, and $MeNO_2$), just as in the non-HBD solvents, the formation of **4** is precluded because of the absence of an acidic proton.

3.2.3. Kinetic Isotope Effect (KIE). Isotope-labeling experiments carried out in the solvent pairs CH_3OH-CD_3OD and $C_2H_5OH-C_2D_5OD$ by the standard GC method demonstrated significant inverse secondary KIEs ($k_H/k_D = 0.80$ and 0.78, respectively) for the rate-controlling first step of the Meisenheimer rearrangement of *N*-oxide **1**. These experiments proved that there is no observable difference in the kinetic parameters measured in aprotic deuterated or aprotic nondeuterated solvents. However, in the case of deuterium oxide, we corrected the measured reaction rate constant by multiplying by a factor of 0.78 due to the observed secondary isotope effect.

Deuterated strong HBD solvents exert two effects on the reaction. When the reaction was performed in deuterated strong HBD solvents, 70−80% of the exchangeable C(sp)−H(10) exchanged to D(10) (the NMR signal of H(10) rapidly decreased to 20−30% of its original value),[15] which influenced the rate-determining step. It is known[62] that such a KIE may be detected if a change in the geometry from sp^2 to sp^3 hybrid states occurs during the reaction. Although to the best of our knowledge there are no relevant literature data, it is reasonable to assume that the present inverse secondary KIE is a consequence of a novel type of hybridization that changes from sp to sp^2, affecting the terminal C(10) sp atom of the propargyl group of *N*-oxide **1** as reaction center. If we suppose that H(10) → D(10) exchange occurs for **1**, we can estimate the KIE from a simple theoretical description (eq 14),[62] where only the average IR frequencies of C(sp)−H of *N*-oxide **1** and those of C(sp^2)−H of TS **2** are considered. The calculation gave practically the same result as the experiments.

$$\frac{k_H}{k_D} = \frac{\exp\left\{\frac{0.7195}{T}\sum_{i=1}^{3n_A-6}[\nu_i(AH) - \nu_i(AD)]\right\}}{\exp\left\{\frac{0.7195}{T}\sum_{i=1}^{3n^{\mp}-7}[\nu_i(H)^{\mp} - \nu_i(D)^{\mp}]\right\}} =$$

$$= \frac{\exp\left\{\frac{0.7195}{T}[\nu(AH) + 2\delta(AH) - \nu(AD) - 2\delta(AD)]\right\}}{\exp\left\{\frac{0.7195}{T}[\nu(H)^{\mp} + \delta_1(H)^{\mp} + \delta_2(H)^{\mp} - \nu(D)^{\mp} - \delta_1(D)^{\mp} - \delta_2(D)^{\mp}]\right\}} =$$

$$= \frac{\exp\left[\frac{0.7195}{338}(3300 + 2\cdot630 - 2444 - 2\cdot467)\right]}{\exp\left[\frac{0.7195}{338}(3020 + 1300 + 810 - 2237 - 963 - 600)\right]} = 0.73 \qquad (14)$$

In eq 14, k_H and k_D denote the reaction rate constants in nondeuterated and deuterated solvents, respectively, ν_i is the IR frequencies of molecules containing hydrogen or deuterium, ν(AH), ν(AD), δ(H), and δ(D) are the bond stretching and bending frequencies of the C−L group (L = H or D) for structure **1** (estimated from literature data for propargyl groups), and $\nu(AH)^{‡}$, $\nu(AD)^{‡}$, $\delta_1(H)^{‡}$, and $\delta_2(H)^{‡}$ are the bond stretching and bending frequencies of TS **2** (estimated from literature data for molecules containing a similar bond pattern, >C═CL−O).

The second effect of deuterated solvents on this reaction appears during the protonation process **5*** → **6***, where a proton binds to C(9) of **5*** (Scheme 2). In deuterated solvents, deuterium atom takes part in this process, and the resulting **4** contains a deuterium on C(9)[15] in addition to that on C(10). This process influences only the product distribution step and has no effect on the examined rate-controlling step.

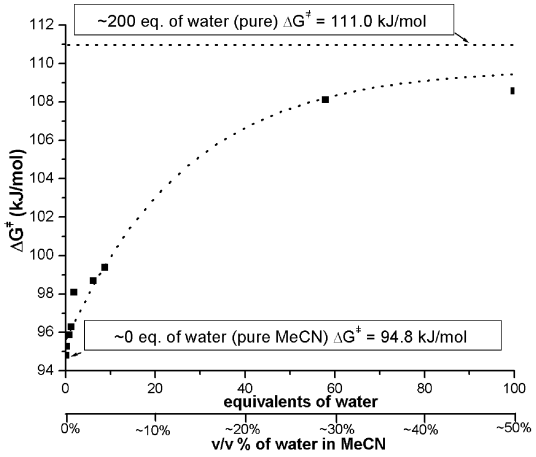

Figure 7. Increase in $\Delta G^{‡}_{OBS}$ values calculated for the rearrangement of *N*-propargylmorpholine *N*-oxide (**1**) in MeCN solutions on the addition of different amounts of water (see text for experimental conditions).

3.2.4. Titration with EPA and Water in MeCN. To demonstrate the role of HB in decreasing the rate of the rearrangement of *N*-oxide **1**, we carried out titration experiments with standard MeCN solutions, adding different amounts of water to the reaction mixture (0.1, 0.3, 0.8, 1.3, 1.9, 6.2, 8.8, 58, and 100 molar equiv as compared with the substrate). We found a significant decrease in the reaction rate, which undoubtedly indicates the effect of HB. For example, 1.9 equiv of water (ca. 0.7%) reduced the reaction rate to one-fifth, and the rate in a 1:1 (v/v) mixture of MeCN and water (100 equiv) almost reached the rate observed in pure water. Figure 7 illustrates the increase in the free energy of activation during titration relating to "solvent sorting" or "selective solvation".[63,64] The calculated $\Delta G^{‡}_{OBS}$ changed from 94.8 kJ mol^{-1} (pure MeCN) to 111.0 kJ mol^{-1} (pure water) during titration. This type of experiment is suitable to determine the water concentration when the 1:1 complex formed between the *N*-oxide and water predominates (see Section 3.3.4). The fitted curve is proportional to a ln function that relates to the dependence of $\Delta G^{‡}_{OBS}$ on ln([H_2O]) (see Section 1.3).[63,64]

Product **4**, which forms in protic (strong HBD) media, appears only in the 2:1 mixture of MeCN/H_2O (ca. 60 equiv of water as compared to **1**). In the case of the higher water content, this compound did not even form at below 10 equiv of water (ca. 3.0 v/v%). The product ratio [**3**]/[**4**] is unpredictable because of the following degradation steps.

HBD molecules belong to the larger family of EPAs. Hence, similar rate-reducing effects can be expected from other known EPA molecules. In the present study, certain aromatic compounds (such as pyridine, different nitro derivatives of benzene), $LiClO_4$, $NaClO_4$, BF_3:OEt_2, and HCl were investigated as shown in Table 4.

BF_3 and H^+ proved to be the strongest EPA additives since the addition of 1 equiv of BF_3 or H^+ practically halted the reaction. One equivalent of Li^+ decreased the rate to ap-

(62) Ruff, F.; Csizmadia, I. G. *Organic Reactions: Equilibria, Kinetics and Mechanism*; Elsevier: Amsterdam, 1994; Chapter 8, pp 232−239.
(63) Abboud, J.-L. M.; Douhal, A.; Arin, M. J.; Diez, M. T.; Homan, H.; Guihéneuf, G. *J. Phys. Chem.* **1989**, *93*, 214−220.
(64) Marcus Y. In *Solvent Mixtures: Properties and Selective Solvation*; Marcel Dekker: New York, 2002; Chapter 5, pp 180−234.

Table 4. Rate Constants and $\Delta G^{\ddagger}_{OBS}$ Values Obtained for the Rearrangement of *N*-Propargylmorpholine *N*-Oxide (**1**) in MeCN Solutions Containing EPA Molecules (for Experimental Conditions, See Text)

EPA	EPA added[a]	T (K)	k (s^{-1})	k^o (s^{-1})[b]	k_{rel}	$\Delta G^{\ddagger}_{OBS}$ (kJ mol^{-1})
H^+	1	343	0[c]	0	0	−
BF_3	1	343	0[c]	0	0	−
$LiClO_4$	0.8	343	7.35×10^{-4}	1.98×10^{-5}	0.023	104.3
$LiClO_4$	1	343	7.69×10^{-4}	2.07×10^{-5}	0.024	104.2
$LiClO_4$	2	343	5.09×10^{-4}	1.32×10^{-5}	0.015	105.4
$LiClO_4$	5	352	4.39×10^{-4}	3.72×10^{-6}	0.0043	108.6
$NaClO_4$	1	343	4.34×10^{-3}	1.38×10^{-4}	0.16	99.3
$NaClO_4$	2	343	2.16×10^{-3}	6.42×10^{-5}	0.075	101.3
$NaClO_4$	5	343	8.43×10^{-4}	2.29×10^{-5}	0.027	103.9
1 equiv of TNB[e]	1	323	2.03×10^{-3}	6.46×10^{-4}	0.75	95.5
2 equiv of TNB[e]	2	323	1.98×10^{-3}	2.50×10^{-4}	0.29	96.0
cc.TNB[e]	∼10	338	2.89×10^{-4}	1.29×10^{-4}	0.15	105.4
1 equiv of DNB[d]	1	323	2.78×10^{-3}	7.92×10^{-4}	0.92	95.1
2 equiv of DNB[d]	2	323	1.97×10^{-3}	6.11×10^{-4}	0.71	95.6
cc.DNB[d]	∼10	338	5.92×10^{-4}	2.84×10^{-5}	0.033	103.4
$PhNO_2$	p.s.[f]	313	1.31×10^{-3}	1.31×10^{-3}	1.52	93.8
pyridine	p.s.[f]	309	9.73×10^{-4}	1.54×10^{-3}	1.79	93.4
MeCN[g]	**p.s.[f]**	**313**	$\mathbf{8.61 \times 10^{-4}}$	$\mathbf{8.61 \times 10^{-4}}$	**1.00**	**94.8**

[a] Equivalent amount of EPA as compared with *N*-oxide **1**. [b] Calculated for 313 K. [c] Not measurable. [d] 1,3-Dinitrobenzene (DNB). [e] 1,3,5-Trinitrobenzene (TNB). [f] Pure solvent. [g] Reference solvent.

proximately the same extent as observed in alcoholic solutions ($k_{rel} = 0.023$, $\Delta G^{\ddagger}_{OBS} = 104.3$ kJ mol^{-1}), although the molar ratio of complexing ROH and *N*-oxygen is much larger in the latter case, as it appeared that two ROH molecules were coordinated to the *N*-oxygen instead of one species (see Section 3.3.4). The rate-decreasing effect of Na^+ is approximately 1 order of magnitude weaker ($k_{rel} = 0.16$, $\Delta G^{\ddagger}_{OBS} = 99.3$ kJ mol^{-1}) than that of Li^+.

Our data reveal that only saturated solutions of 1,3,5-trinitrobenzene (TNB) and 1,3-dinitrobenzene (DNB) (200 mg/750 μL; ∼10 equiv) have such effects on the protic solvents ($k_{rel} = 0.015$ and 0.033, $\Delta G^{\ddagger}_{OBS} = 105.4$ and 103.4 kJ mol^{-1}, respectively). TNB displays a larger rate-decreasing effect than DNB, but TNB is only in a concentrated solution as effective as *t*-BuOH or *i*-PrOH. One equivalent amount of TNB decreases the rate only 0.75-fold; this effect is similar to that of 1 equiv of ROH in a standard solution. Nitrobenzene and pyridine could be investigated only as pure solvents. They acted as very weak EPAs, but the effects are negligible. The rate-decreasing effects of various EPAs and HBDs on $\Delta G^{\ddagger}_{OBS}$ for the rearrangements of *N*-oxide **1** are depicted in Figure 8.

Comparison of the titration curves of the EPAs (Li^+, Na^+, DNB, and TNB) and water (Figure 9) allows the conclusion that Li^+ and Na^+ reach their saturation point near 5 equiv, while the weaker DNB and TNB do not attain their maximum effect even at 10 equiv. The water curve lies between the pairs Li^+/Na^+ and DNB/TNB, demonstrating a moderate EPA effect. Saturation is reached at around 2−3 equiv.

The presence of different EPAs in non-HBD MeCN solutions has a significant effect on the rate reduction, but the lack of protonating ability of these species means that product **3** is formed exclusively. This is connected with their single function (see Section 1.3) relative to the weak HBD solvents ($CHCl_3$, CH_2Cl_2, and $CHBr_3$).

3.2.5. Energetic and Mechanistic Concepts. The results observed for the rate constant and product ratio can be related to the dual function of the strong HBD (protic) solvents, the single function of the weak HBD and EPA molecules, and the zero function of the non-HBD (aprotic) solvents. The experimental data indicate large differences in reaction rates and free

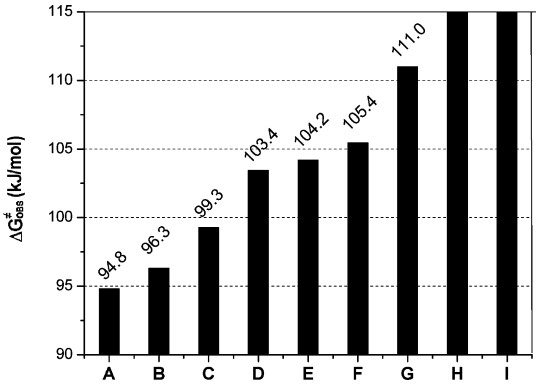

Figure 8. Effects of EPAs and HBDs on $\Delta G^{\ddagger}_{OBS}$ values for the rearrangement of *N*-propargylmorpholine *N*-oxide (**1**) in different solvents. (A) Pure MeCN. (B) 1 equiv of H_2O in MeCN. (C) 1 equiv of Na^+ in MeCN. (D) Concentrated DNB−MeCN solution. (E) 1 equiv of Li^+ in MeCN. (F) Concentrated TNB−MeCN solution. (G) Pure H_2O. (H) 1 equiv of BF_3:OEt_2 in MeCN. (I) 1 equiv of H^+ in MeCN.

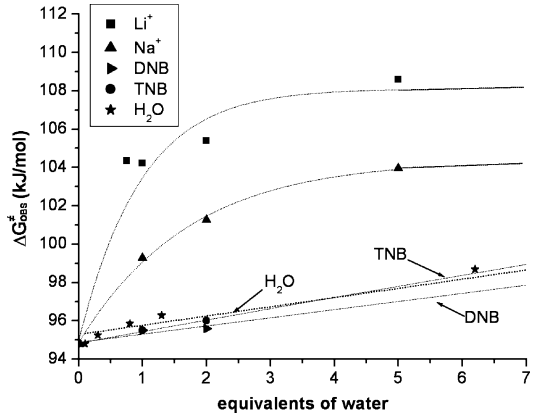

Figure 9. Comparison of the titration curves of different EPAs and water.

energies of activation when *N*-oxide **1** is transformed in solvents belonging to different classes. Extreme Δk_{rel} values ($\Delta k_{rel} = 8.71 \times 10^{-4}$, corresponding to $\Delta\Delta G^{\ddagger}_{OBS} = 18.6$ kJ mol^{-1}) characterize such reactions as those conducted in dioxane (type 1) or water (type 2B). On the other hand, the differences between the solvents are rather small within a given class ($\Delta\Delta G^{\ddagger}_{OBS} =$ 1−6 kJ mol^{-1}). If the series of different solvents are considered,

Table 5. Computed Activation Parameters (kJ mol^{-1}) and Atomic Distances (Å) Obtained with the Implicit Solvent Model (1) for the Rearrangement of *N*-propargylmorpholine *N*-oxide (**1**) in Different Solvents, as Compared with the Experimental Data (2)

	implicit method (1)										experiment (2)		$\Delta\Delta G^{\ddagger}$
solvent	solvent type[a]	$\Delta E^{\ddagger}$	$\Delta E^{\ddagger}_{CORR}$ [b]	$\Delta H^{\ddagger}_{CORR}$ [b]	$\Delta G^{\ddagger}_{CORR}$ [b,c]	$\Delta H^{\ddagger}_{CPE}$ [d]	$\Delta G^{\ddagger}_{CPE}$ [c,d]	$\Delta H^{\ddagger}_{TOT}$ [e]	$\Delta G^{\ddagger}_{TOT}$ [c,e]	*d* (O···C)[f]	$\Delta H^{\ddagger}_{OBS}$	$\Delta G^{\ddagger}_{OBS}$	(1) – (2)
H_2O	2B	83.95	85.9	84.36	89.06	2.93	3.25	87.29	92.31	2.05	107.3	111.0	−18.69
MeOH	2B	83.73	85.68	84.03	88.73	3.46	3.61	87.49	92.34	2.05	105.0	109.7	−17.36
EtOH	2B	82.86	84.81	83.18	87.88	4.12	4.27	87.3	92.15	2.05	103.7	108.6	−16.45
CF_3CH_2OH[g]	2B	82.86	84.81	83.18	87.88	4.12	4.27	87.3	92.15	2.05	104.5	110.4	−18.25
i-PrOH	2B	82.63	84.58	83.01	87.71	4.21	4.47	87.22	92.18	2.05	101.0	106.8	−14.62
$(CF_3)_2CHOH$[g]	2B	82.63	84.58	83.01	87.71	4.21	4.47	87.22	92.18	2.05	104.8	110.9	−18.72
t-BuOH	2B	81.29	83.24	81.62	86.32	5.15	5.09	86.77	91.41	2.05	97.6	104.6	−13.19
CH_2Cl_2	2A	80.49	82.44	80.87	85.57	5.45	5.47	86.32	91.04	2.05	90.0	96.0	−4.96
$CHCl_3$	2A	77.19	79.14	75.41	80.11	6.74	6.73	82.15	86.84	2.06	92.9	98.8	−11.96
$MeNO_2$	2A	83.76	85.71	84.10	88.8	3.41	3.66	87.51	92.46	2.05	90.7	96.6	−4.14
Me_2SO	1	83.83	85.78	84.19	88.89	3.47	3.75	87.66	92.64	2.05	90.0	95.9	−3.26
MeCN	1	83.74	85.69	84.08	88.78	3.44	3.69	87.52	92.47	2.05	89.0	94.8	−2.33
$PhNO_2$	1	83.68	85.63	84.05	88.75	3.44	3.65	87.49	92.4	2.05	87.9	93.8	−1.40
Me_2CO	1	82.63	84.58	83.01	87.71	4.21	4.47	87.22	92.18	2.06	87.0	92.9	−0.72
pyridine	1	81.40	83.35	81.51	86.21	4.98	4.82	86.49	91.03	2.06	87.6	93.4	−2.37
dioxane	1	72.74	74.69	73.32	78.02	8.86	8.67	82.18	86.69	2.07	83.1	89.1	−2.41
in vacuo[h]	1	66.75	68.7	67.39	72.09	10.30	9.70	77.69	81.79	2.04			

[a] 1: Non-HDBs, 2A: weak HDBs, 2B: strong HDBs. [b] Including ZPE and BSE. [c] Estimated from $\Delta H^{\ddagger}$ on the assumption that $\Delta S^{\ddagger}$ (−14.61 J mol^{-1} K^{-1}) is constant in different solvents. [d] Difference between the gauche and anti conformers (pre-equilibrium). [e] With consideration of BSE, dispersion, and pre-equilibrium effect. [f] O(7)···C(10) atomic distance in TS **2**. [g] Calculated data equal to those computed for EtOH and *i*-PrOH, respectively. [h] Taken from ref 17.

a decrease in the rate of reaction and an increase in the free energy of activation can be observed on increase of the polarity of the solvent according to the theoretical Kirkwood−Onsager rules.[23,56]

The data obtained on HBD solvents (types 2A and 2B) reveal the relative importance of the solvent polarity and the ability of HBD to control the rate of reaction. The relative permittivities (ϵ_{rel}) of MeCN and MeOH are comparable, whereas the $\Delta G^{\ddagger}_{OBS}$ values determined for the rearrangements differ markedly (ϵ_{rel} = 35.94 and 32.66; $\Delta G^{\ddagger}_{OBS}$ = 94.8 and 109.7 kJ mol^{-1}, respectively). The situation is similar when the solvents Me_2CO, *i*-PrOH, and $(CF_3)_2CHOH$ are compared (ϵ_{rel} = 20.70, 19.92, and ∼20; $\Delta G^{\ddagger}_{OBS}$ = 92.9, 106.8, and 108.2 kJ mol^{-1}, respectively). The reaction rate in CH_2Cl_2 is somewhat smaller than those in aprotic solvents (e.g., in Me_2CO) that have similar relative permittivities. The relative $k(Me_2CO)/k(CH_2Cl_2)$ value of 3.23 points to a moderate rate-reducing effect of very weak HB between CH_2Cl_2 and *N*-oxide **1** molecules. It may be concluded unequivocally that the marked decrease in reaction rate is due to the HBD ability of the solvents.

The three types of solvents (types 1, 2A, and 2B) each exhibit different behavior. Non-HBD solvents give only one intermediate in a rapid reaction. The kinetic data revealed that strong HBD solvents and EPA molecules could be substituted for each other. Both of them gave rise to similar rate-decreasing effects, but EPA molecules have only a single functionality, which does not permit formation of the non-Meisenheimer product (**4**), due to the absence of the exchangeable proton that is essential in step **5*** → **6***. Protic solvents allow the formation of **4***, which results in a lower reaction rate as compared with other solvent types.

3.3. Computational Kinetics. 3.3.1. Calculations in the Gas Phase and in Non-HBD Solvents (in Vacuo and PCM Model). As mentioned earlier, the computed activation parameters of the RC step of the rearrangement of *N*-oxide **1** in vacuo are as follows: $\Delta E^{\ddagger}_{RC}$ = +66.7 kJ mol^{-1}, $\Delta H^{\ddagger}_{RC}$ = +65.4 kJ mol^{-1}, $\Delta G^{\ddagger}_{RC}$ = +69.7 kJ mol^{-1}, and $\Delta S^{\ddagger}_{RC}$ = −14.61 J mol^{-1} K^{-1}. When CPE and BSE are included, the calculated $\Delta G^{\ddagger}_{TOT}$ of +81.79 kJ mol^{-1} is close to the value measured in dioxane ($\Delta G^{\ddagger}_{OBS}$ = 92.9 kJ mol^{-1}, see Table 5), but seems very low in comparison with the value ($\Delta G^{\ddagger}_{OBS}$ = 111.0 kJ mol^{-1}, see Table 5) obtained experimentally in aqueous solvents. The very large difference in the case of water does not stem from the low efficiency of the theoretical methods, but is rather due to the inappropriate application of chemical modeling to HB.

However, the relatively small deviations point to the influence of the relative permittivities (ϵ_{rel}) of the solvent molecules, which are present in large amount under the experimental conditions. To model aprotic solvents, we chose the PCM method[1−4] from the implicit solvation method family. Using the implicit PCM model, we first calculated the energies of the *N*-oxide **1** conformers in different solvents, including the activation parameters for the conformational anti/gauche equilibrium reaction. Data indicative of a significant solvent dependence are found in Table 5 (see columns $\Delta H^{\ddagger}_{CPE}$ and $\Delta G^{\ddagger}_{CPE}$).

To obtain the corrected activation parameters ($\Delta E^{\ddagger}_{CORR}$, $\Delta H^{\ddagger}_{CORR}$, and $\Delta G^{\ddagger}_{CORR}$), we used eqs 15−19 for the PCM models:

$$\Delta E^{\ddagger}_{CORR} = \Delta E^{\ddagger} + \Delta E^{\ddagger}_{BSE} = \Delta E^{\ddagger} + 1.95 \text{ kJ mol}^{-1} \quad (15)$$

$$\Delta H^{\ddagger}_{CORR} = \Delta H^{\ddagger} + \Delta E^{\ddagger}_{BSE} = \Delta H^{\ddagger} + 1.95 \text{ kJ mol}^{-1} \quad (16)$$

$$\Delta G^{\ddagger}_{CORR} = \Delta H^{\ddagger}_{CORR} - T\Delta S^{\ddagger}_{CORR} = \Delta H^{\ddagger}_{CORR} - (-14.24 \text{ J K}^{-1} \text{ mol}^{-1})\cdot T \quad (17)$$

The final (TOT) activation parameters are composed of two terms related to CPE and the correction introduced previously (CORR).

$$\Delta H^{\ddagger}_{TOT} = \Delta H^{\ddagger}_{CORR} + \Delta H_{CPE} \quad (18)$$

$$\Delta G^{\ddagger}_{TOT} = \Delta G^{\ddagger}_{CORR} + \Delta G_{CPE} \quad (19)$$

In applying the PCM model, we calculated the activation parameters for rearrangement of *N*-oxide **1** in all the solvents

Table 6. Computed Activation Parameters (kJ mol^{-1}) and Atomic Distances (Å) Obtained with the Explicit (1) and the Explicit−Implicit Solvent Model (2) for the Rearrangement of *N*-Propargylmorpholine *N*-Oxide (**1**) in Different Solvents, as Compared with the Experimental Data (3)

	explicit method (1)					explicit–implicit method (2)				experiment (3)		$\Delta\Delta G^{\ddagger}$	$\Delta\Delta G^{\ddagger}$
solvent	solvation[a]	$\Delta E^{\ddagger}_{CORR}$ [b]	$\Delta H^{\ddagger}_{TOT}$ [c]	$\Delta G^{\ddagger}_{TOT}$ [c,d]	d (O···C)[e]	$\Delta E^{\ddagger}_{CORR}$ [b]	$\Delta H^{\ddagger}_{TOT}$ [c]	$\Delta G^{\ddagger}_{TOT}$ [c,d]	d (O···C)[e]	$\Delta H^{\ddagger}_{OBS}$	$\Delta G^{\ddagger}_{OBS}$	(1) − (3)	(2) − (3)
H_2O	1	88.08	89.06	94.45	1.87	93.18	94.16	99.55	1.96	107.3	111.0	−16.55	−14.45
	2	103.93	105.75	110.97	1.78	104.41	106.23	111.45	1.88			−0.03	0.45
MeOH	1	88.17[f]	89.29	94.51	1.88					105	109.7	−16.46	
	2	103.65[f]	105.18	110.4	1.79	104.11	105.64	110.86	1.92			0.7	1.16
EtOH	1	87.30	88.11	93.33	1.88					103.7	108.6	−16.55	
	2	103.58	105.54	110.76	1.80	103.13	105.09	110.31	1.92			2.16	1.71
CF_3CH_2OH	2	115.58	117.32	122.54	1.75	116.01	117.75	122.97	1.85	104.5	110.4	12.44	12.57
i-PrOH	1	88.18	89.83	94.3	1.88					101.0	106.8		
	2	102.87	104.52	109.85	1.84	101.83	103.48	108.81	1.93			3.05	2.01
$(CF_3)_2CHOH$	2	121.22	122.73	127.21	1.79	119.35	120.91	126.24	1.85	104.8	110.9	16.30	15.34
t-BuOH	1	87.79	88.99	94.00	1.89	90.87	92.07	97.08	1.92	97.6	104.6		−7.52
	2	102.01	103.54	108.55	1.84	101.1	102.63	107.64	1.92			3.95	3.04
CH_4	1	70.56	70.77	75.99	2.02	85.58	85.79	91.01	2.05				
$MeNO_2$	1	85.38	82.27	92.11	1.93	88.61	84.28	95.34	2.02	90.7	96.6	−4.49	−1.26
CH_2Cl_2	1	84.85	87.35	92.44	1.93	87.8	90.3	95.39	2.01	90.0	96.0	−3.56	−0.61
	2	93.79	94.29	99.38	1.89							3.38	-
$CHCl_3$	1	87.15	90.94	96.00	1.9	89.17	92.96	98.02	1.98	92.9	98.8	−2.8	−0.78
	2	96.30	99.09	104.15	1.84							−5.35	

[a] Number of solvent molecules. [b] Including ZPE and BSE. [c] With consideration of BSE, dispersion, and pre-equilibrium effect. [d] Estimated from $\Delta H^{\ddagger}$ on the assumption that $\Delta S^{\ddagger}$ (−14.61 J mol^{-1} K^{-1}) is constant in different solvents. [e] O(7)···C(10) atomic distance in the TS **2**. [f] Using $\Delta E^{\ddagger}$ data taken from ref 17.

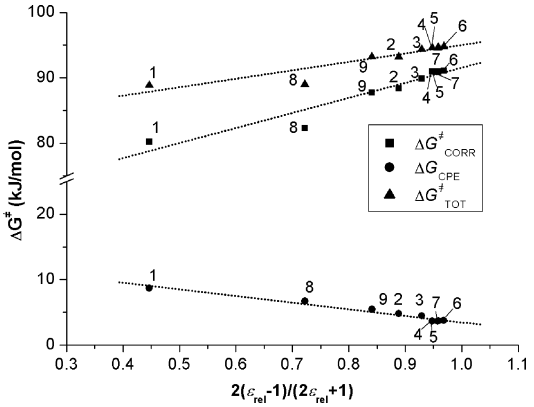

Figure 10. Dependence of $\Delta G^{\ddagger}_{CORR}$, ΔG_{CPE}, and $\Delta G^{\ddagger}_{TOT}$ (see eqs 15−19) on the relative permittivities of the solvents used, as calculated with the implicit solvent model (IEF-PCM) for the rearrangement of *N*-propargylmorpholine *N*-oxide (**1**). 1: dioxane. 2: pyridine. 3: Me_2CO. 4: $PhNO_2$. 5: MeCN. 6: Me_2SO. 7: $MeNO_2$. 8: $CHCl_3$. 9: CH_2Cl_2.

used in the kinetic measurements. The data in Table 5 indicate that the calculated $\Delta G^{\ddagger}_{TOT}$ values for non-HBD solvents are very close to the measured ones [$\Delta\Delta G^{\ddagger} = (-0.72) - (-3.26)$ kJ mol^{-1}], whereas the data for strong HBD (type 2B) solvents [$\Delta\Delta G^{\ddagger} = (-18.72) - (-13.19)$ kJ mol^{-1})] differ significantly. Weak HBD solvents (type 2A) exhibit intermediate deviations [$\Delta\Delta G^{\ddagger} = (-4.96) - (-11.96)$ kJ mol^{-1}].

Figure 10 depicts the dependence of the calculated $\Delta G^{\ddagger}$ data ($\Delta G^{\ddagger}_{TOT}$, $\Delta G^{\ddagger}_{CPE}$, and $\Delta G^{\ddagger}_{RC}$) on the relative permittivities according to the Kirkwood−Onsager rule [$2(\epsilon_{rel} - 1)/(2\epsilon_{rel} - 1)$][23,56] for different (non-HBD and weak HBD) solvents. All ΔG values ($\Delta G^{\ddagger}_{TOT}$, $\Delta G^{\ddagger}_{CPE}$, and $\Delta G^{\ddagger}_{RC}$) are in good agreement with the Kirkwood−Onsager rules, but $\Delta G^{\ddagger}_{CPE}$ and $\Delta G^{\ddagger}_{RC}$ have opposite slopes, demonstrating conflicting changes with the dipole moment in the processes **1b** → **1c**/**1d** and **1c**/**1d** → **2**.

3.3.2. Kinetics in HBD Solvents (Explicit and Joint Explicit and Implicit Solvent Models). (A) Calculations with Explicit Solvent Model. MD studies allow the conclusion that two strong HBD or one weak HBD solvent molecules form the first shell at a given reaction temperature for the rearrangement of **1**. We investigated the activation energy calculations with one and two of the explicit solvent molecules listed in Table 6 to verify our prediction. As may be seen from Table 6, the computed $\Delta G^{\ddagger}_{TOT}$ of the explicit−implicit values confirmed the experimental $\Delta G^{\ddagger}_{TOT}$ results.

The solvent molecules may assume different conformations. We chose the conformers with lowest energy, estimating the conformational energies by using the B3LYP/6-31G(d) method. Direct computation of the activation entropy is impossible because of the many low-frequency motions originating from the solvent molecules; accordingly, the value of $\Delta S^{\ddagger}_{CORR}$ (−14.61 J mol^{-1} K^{-1}) was used, as introduced in Section 2.2.3.

The $\Delta G^{\ddagger}_{TOT}$ values were calculated in the same way as described for the implicit method in eqs 15−17. The values of ΔG_{CPE} in different solvents were considered to be equal to those obtained with the implicit model.

Table 6 lists the activation parameters calculated with the explicit model in the solvents H_2O, MeOH, EtOH, CF_3CH_2OH, *i*-PrOH, $(CF_3)_2CHOH$, *t*-BuOH, $CHCl_3$, CH_2Cl_2, and $MeNO_2$, where one or two solvent molecules form a solvation complex with the negatively charged oxygen in *N*-oxide **1**. Extreme $\Delta G^{\ddagger}_{TOT}$ data can be observed for the fluorinated solvents, which yielded the largest deviations from the experimental values. These solvents comprise a separate group in the family of strong HBD solvents. In nonfluorinated solvents, $\Delta\Delta G^{\ddagger}$ values of less than 3.95 kJ mol^{-1} reveal that the explicit solvent model is more capable of describing a protic (HBD) solvent effect than the implicit variation.

The $\Delta G^{\ddagger}_{TOT}$ values computed by using the explicit solvent models were individually quite close to those measured experimentally for HBD solvents. The trend is undoubtedly similar to that observed in the experiments where the $\Delta G^{\ddagger}_{TOT}$ values decreased with increase of the relative permittivities of the strong HBD solvents, with the exception of fluorinated solvents. It is striking, however, that the relative $\Delta G^{\ddagger}_{TOT}$ values [$\Delta G^{\ddagger}_{TOT}$(ROH) − $\Delta G^{\ddagger}_{TOT}$($H_2O$)] calculated for different protic

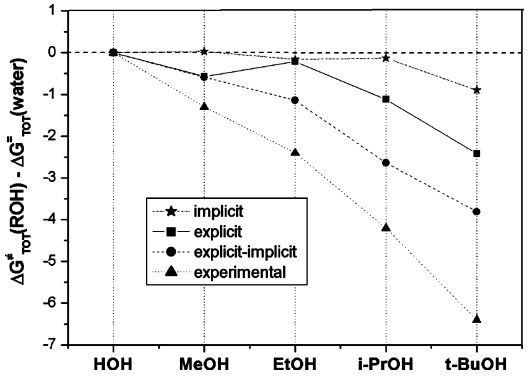

Figure 11. Comparison of the differences $\Delta G^{\ddagger}_{TOT}(ROH) - \Delta G^{\ddagger}_{TOT}(H_2O)$ obtained from the implicit, explicit, and explicit−implicit solvent models with the experimental results.

solvents were smaller than the differences between the experimental ones. In the solvent series from water to *t*-BuOH, the computed relative $\Delta G^{\ddagger}_{TOT}$ value is only 2.42 kJ mol^{-1}, while it was measured to be 6.40 kJ mol^{-1} (Figure 11). This marked deviation may be a result of the dominating HB and the neglect of the relative permittivities of the solvents in controlling the rate of rearrangement of *N*-oxide **1** when the explicit solvent model is used.

Calculations for different protic and HBD solvents gave the atomic distances between the reacting O(7) and C(10) atoms, that is, the negatively charged *N*-oxygen and the terminal C atom of the propargyl group in TS **2**, as 1.75 (CF_3CH_2OH), 1.84 (*t*-BuOH), 1.90 ($CHCl_3$), and 1.93 Å (CH_2Cl_2) (Table 6). This means that TS **2** in CF_3CH_2OH was the farthest and CH_2Cl_2 was the nearest to the substrate state, which is in accordance with the relative reaction rates. The atomic distances in HBs of different strengths, calculated for the various protic solvents, were also in agreement with the different reactivities of the *N*-oxide complexes. It may be concluded that the explicit solvent model, in contrast with the implicit model, affords acceptable results in describing the reactivity in different protic solvents. Still, the exclusive role of the HBs in controlling the reactivities may be criticized. For fluorinated solvents, the large activation energies can be explained by the strong HB abilities of these solvents, which is reflected in the O(7)−C(10) distance. The agreement between the experimental and computed values is weak, demonstrating an additional solvent effect.

(B) Calculations with Joint Explicit−Implicit Solvent Model. The explicit solvent model takes into account only the effects of HB, other solvent effects, such as the relative permittivities on which the implicit PCM model is based, being neglected. From the results obtained separately with the implicit and explicit models, we concluded that a suitable way to obtain correct activation parameters is joint application of the two methods. Unfortunately, the joint method has the serious disadvantage that the convergence of the optimization process becomes very labile and occasionally turns into an oscillating cycle that requires a considerable amount of calculation time. On the other hand, application of the joint method leads to accurate and realistic results. Table 6 summarizes the data obtained and demonstrates better agreement with the experimental data than for the explicit solvent model alone.

Relative $\Delta G^{\ddagger}_{TOT}$ values less than 3.04 kJ mol^{-1} reveal that the joint model describes the strong HBD solvent effect well. In the series from H_2O to *t*-BuOH, omitting the fluorinated solvents, the relative $\Delta G^{\ddagger}_{TOT}$ values between the two extreme data are 2.42, 3.81, and 6.4 kJ mol^{-1}, as computed with the explicit solvent model or the joint model and measured experimentally, respectively (Figure 11). The largest deviation in relative $\Delta G^{\ddagger}_{TOT}$ was observed for *t*-BuOH, where the solvent model with two solvent molecules is an overestimate, and the solvent model with one solvent molecule is an underestimate of the experimental value. With reference to the MD study, the experimental value can be estimated from a consideration of the models with one or two *t*-BuOH molecules.

In Figure 12, the $\Delta G^{\ddagger}$ values obtained experimentally and the $\Delta G^{\ddagger}_{TOT}$ calculated for the rearrangement of *N*-oxide **1** with the implicit and joint implicit−explicit methods are shown in different solvents, depending on the relative permittivities.

The similar $\Delta\Delta G^{\ddagger}_{TOT}$ values obtained with the explicit and joint explicit−implicit solvent models for protic solvents permit the conclusion that the first solvation shell is involved to the highest degree in the solvent effect.

For fluorinated solvents, the agreement between the experimental and computed values is weak as compared with that for nonfluorinated solvents, indicating the existence of an additional solvent effect that has yet to be described. In these cases, the second solvation shell (−C−F···H−O−) may also

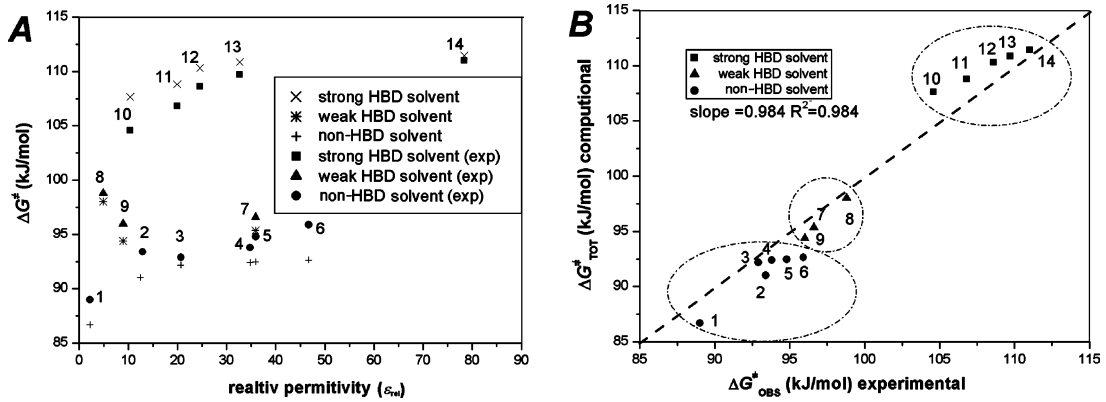

Figure 12. (A) Dependence of $\Delta G^{\ddagger}_{TOT}$ (see eq 19) on the relative permittivities of the solvents used, as measured and calculated with the joint implicit−explicit solvent model for the rearrangement of *N*-propargylmorpholine *N*-oxide (**1**). (B) Correlation between the experimental and theoretical values. 1: dioxane. 2: pyridine. 3: Me_2CO. 4: $PhNO_2$. 5: MeCN. 6: Me_2SO. 7: $MeNO_2$. 8: $CHCl_3$. 9: CH_2Cl_2. 10: *t*-BuOH. 11: *i*-PrOH. 12: EtOH. 13: MeOH. 14: H_2O.

possibly play a significant role.[65,66] The construction of a more reliable solvation model for further consideration will be required.

3.3.3. Calculated Kinetic Isotope Effect. As estimated in Section 3.2.3, using eq 14, we found that k_H/k_D was indeed 0.73, which is in good agreement with the measured value, despite the fact that only average IR frequencies from the literature were applied. In isotope-labeling experiments involving use of the solvent pairs MeOH−MeOD-d_3 and EtOH−EtOD-d_5, we observed an inverse secondary KIE (k_H/k_D = 0.78 and 0.80, respectively) for the rate-determining RC step (**1** → **2**). To achieve a more accurate determination of KIE, we used the calculated IR frequencies of **1** and TS **2**. On substituting the calculated IR frequencies for nondeuterated and deuterated **1c**/**1d** and **2** into eq 14, we obtained a value of 0.82, which is in very good agreement with the experimental value.

3.3.4. Calculations in Mixed Solvent. The $\Delta G^{\ddagger}$ values for the rearrangement of *N*-oxide **1** can be easily measured for the free form (e.g., in MeCN) and for the 2:1 water−*N*-oxide complex (in H_2O). However, the calculation for mixed H_2O−MeCN solvents required a more sophisticated approach. First, the equilibrium constants for the formation of water−MeCN and different water−*N*-oxide complexes (Scheme 3) were calculated from the heats of formations (see Table 6).

From the equilibrium constants and the initial experimental concentration of **1**, we calculated the distribution of different water−*N*-oxide complexes in various H_2O−MeCN mixtures, as shown in Figure 13A.

By applying the calculated concentrations of water−*N*-oxide complexes (Figure 13A) in different H_2O−MeCN mixtures and using the calculated $\Delta G^{\ddagger}_{TOT}$ values for the free form of the *N*-oxide, 1:1 and 2:1 water−*N*-oxide complexes [$\Delta G^{\ddagger}_{TOT}(0)$ = 92.47, $\Delta G^{\ddagger}_{TOT}(1)$ = 99.55, and $\Delta G^{\ddagger}_{TOT}(2)$ = 111.45 kJ mol^{-1} respectively; see Sections 3.3.1 and 3.3.2], we calculated $\Delta G^{\ddagger}_{AV}$ in different H_2O−MeCN mixtures (Figure 13B,C) by using eqs 20−22:

$$\text{rate} = k_{AV}\{[1] + \lfloor 1^{H_2O} \rfloor + \lfloor 1^{(H_2O)_2} \rfloor\} = k_0[1] + k_1\lfloor 1^{H_2O} \rfloor + k_2\lfloor 1^{(H_2O)_2} \rfloor \quad (20)$$

$$\exp\frac{-\Delta G^{\ddagger}_{AV}}{RT} = \frac{\exp\frac{-\Delta G^{\ddagger}_{TOT}(0)}{RT}[1] + \exp\frac{-\Delta G^{\ddagger}_{TOT}(1)}{RT}[1^{H_2O}] + \exp\frac{-\Delta G^{\ddagger}_{TOT}(2)}{RT}[1^{(H_2O)_2}]}{\{[1] + [1^{H_2O}] + [1^{(H_2O)_2}]\}} \quad (21)$$

$$\Delta G^{\ddagger}_{AV} = -RT\ln\left\{\frac{\exp\frac{-\Delta G^{\ddagger}_{TOT}(0)}{RT}[1] + \exp\frac{-\Delta G^{\ddagger}_{TOT}(1)}{RT}[1^{H_2O}] + \exp\frac{-\Delta G^{\ddagger}_{TOT}(2)}{RT}[1^{(H_2O)_2}]}{\{[1] + [1^{H_2O}] + [1^{(H_2O)_2}]\}}\right\} \quad (22)$$

where k_{AV} and $\Delta G^{\ddagger}_{AV}$ are the calculated average reaction rate and activation free energy in mixed solvents, and [**1**], [**1**^{x}], and [**1***] are the concentrations of *N*-oxide **1**, 1:1 and 2:1 water−*N*-oxide **1** complexes in mixed solvents, respectively.

(65) O'Hagan, D.; Rzepa, H. S. *Chem. Commun.* **1997**, *7*, 645−652.
(66) Guidry, M.; Drago, R. *J. Am. Chem. Soc.* **1973**, *95*, 759−763.

Scheme 3. Equilibria in Mixed H_2O−MeCN Solutions Used for Determination of the Species Distributions[a]

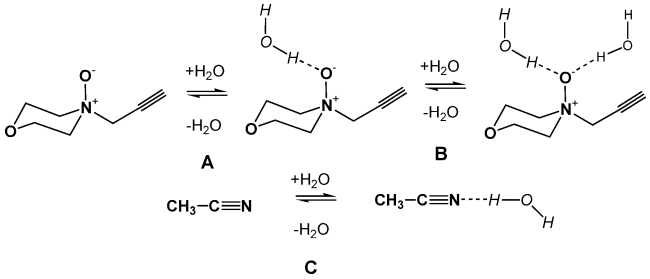

[a] (A) −8.48 kJ mol^{-1}, K_1 = 20.4. (B) −0.34 kJ mol^{-1}, K_2 = 1.14. (C) −0.21 kJ mol^{-1}, K_{ACN} = 1.08; at 323 K.

The concentration of the 1:1 water−*N*-oxide complex reached its maximum at 7 equiv of water (Figure 13) as revealed by the measurements ($\Delta G^{\ddagger}_{TOT}$ = 99.55 kJ mol^{-1} obtained with the joint implicit−explicit method). The slow convergence of the titrated curve to the final value also observed in pure water may be ascribed to the presence of three different components (free *N*-oxide **1**, 1:1 and 2:1 water−*N*-oxide complexes) in the same solution. Thus, the relatively rapid rearrangements of the free form and the 1:1 complex determine the reaction rate in the initial (0−7 equiv of water) and middle (7−60 equiv of water) portions of the titrating curve, respectively.

3.3.5. Effects of Electron-Pair Acceptors. As discussed in Section 3.2.5, measurements carried out in the presence of typical EPA species (DNB, TNB, Na^+, Li^+, BF_3, and H^+) demonstrated a strong decrease in the reaction rates, which can be ascribed to the formation of different complexes between *N*-oxide **1** and EPA additives. The results of the theoretical calculations correlate well with the experimental observations for the Lewis acids Na^+, Li^+, BF_3, and H^+. As is to be seen in Table 7, the calculated activation energies increased in accordance with the strengths of the Lewis acids.

As expected for the ionic complexes of Li^+, Na^+, and H^+ with *N*-oxide **1**, there are large differences between the values calculated in vacuo and with the PCM method. The results obtained with the PCM method are in good agreement with the experimental data. The very high activation energies of the H^+ and BF_3 complexes confirm that that rearrangement does not proceed even at very high temperatures in the presence of only 1 equiv of a strong Lewis acid. The distance between O(7) and C(10) in the TS structure (**2**) decreases in accordance with increasing strength of the Lewis acids, in agreement with the observed activation energies.

For MeCN solutions containing 1 equiv each of Li^+ and Na^+, the calculated $\Delta G^{\ddagger}$ values are higher than those found experimentally. This divergence may be interpreted in terms of the common presence of the free and complexed forms of *N*-oxide **1**. Since the reaction rate for the free form is thousands of times faster than that for the complexed form, even a minimal amount of free *N*-oxide **1** can markedly accelerate the observed reaction rate.

4. Generalized Description of Solvent Effect

As in many other reactions, the overall solvent effect for the overall reaction may be separated into different parts, depending on the consecutive reaction steps (eq 23), composed of ΔG_{CPE}

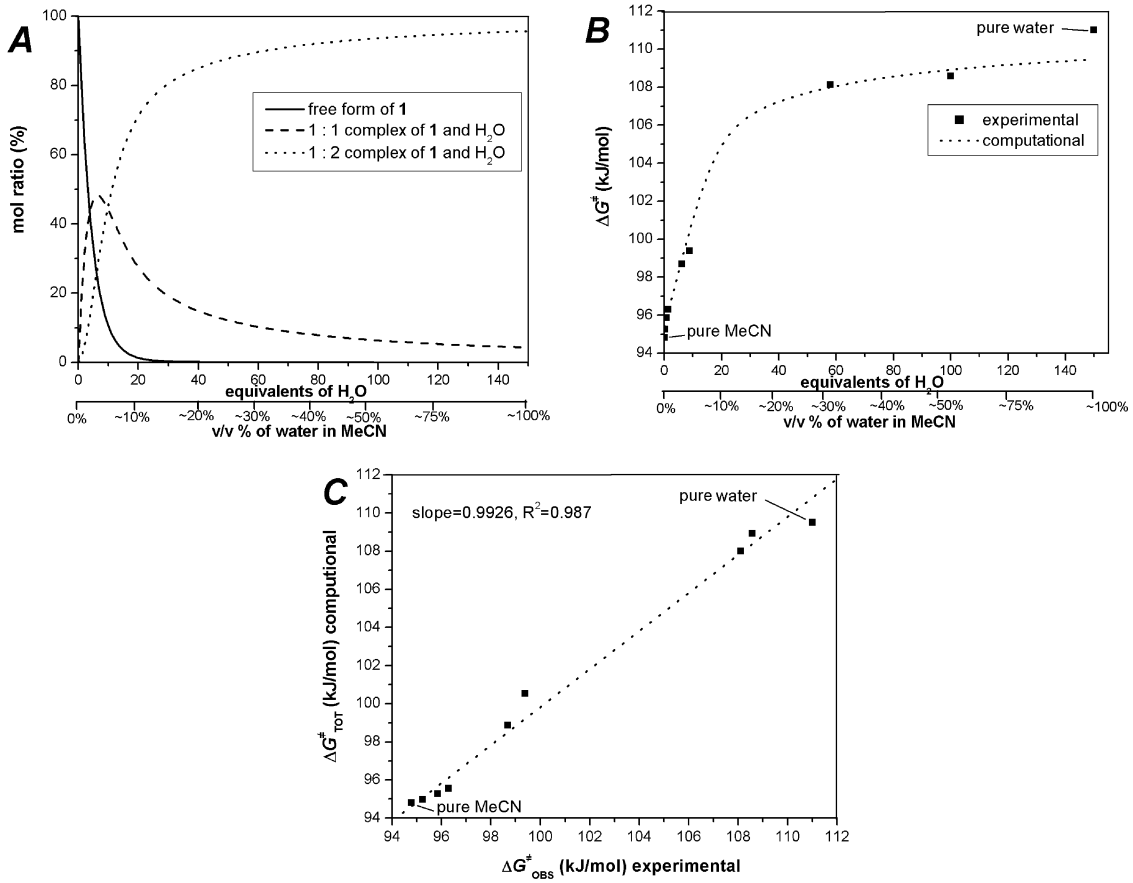

Figure 13. (A) Calculated distribution of different complexes of water−*N*-oxide **1**. (B) The calculated activation energy curve (eqs 20−22) for different water−MeCN mixtures in comparison with the experimental points. (C) Correlation between experimental and theoretical values.

Table 7. Computed Activation Parameters (kJ mol^{-1}) and Atomic Distances (Å) Obtained in Vacuo (1) and with the Implicit Solvent Model (2) for the Rearrangement of *N*-Propargylmorpholine *N*-Oxide (**1**) Dissolved in MeCN Containing EPAs, as Compared with the Experimental Data (3)

	in vacuo (1)			implicit method (2)			experiment (3)		
EPA	$\Delta E^{\ddagger}_{CORR}$ [a]	$\Delta G^{\ddagger}_{TOT}$ [b]	*d* O(7)···C(10)[c]	$\Delta E^{\ddagger}_{CORR}$ [a]	$\Delta\Delta G^{\ddagger}_{TOT}$ [b]	*d* O(7)···C(10)[c]	$\Delta G^{\ddagger}_{OBS}$	$\Delta\Delta G^{\ddagger}$ (1) – (3)	$\Delta\Delta G^{\ddagger}$ (2) – (3)
H^+	185.45	192.61	1.50	217.65	224.81	1.55	n.r.[d]		
BF_3	180.45	187.61	1.80	187.65	194.85	1.55	n.r.[d]		
Li^+	181.75	187.91	1.92	111.75	118.71	1.59	108.6	79.31	10.11
Na^+	157.35	164.51	2.37	99.85	106.83	1.65	103.9	60.61	2.93

[a] Including ZPE and BSE. [b] With consideration of BSE, dispersion, pre-equilibrium, and entropy (−14.61 J mol^{-1} K^{-1}) values. [c] O(7)···C(10) atomic distance in TS **2**. [d] Not recordable.

and $\Delta G^{\ddagger}_{RC}$. Both ΔG values can be correlated with the solvent parameters Π^* and α by using the Kamlet−Taft multilinear regression method (eqs 24 and 25, Table 8):[67,68]

$$\Delta G^{\ddagger}_{sum} = \Delta G_{CPE} + \Delta G^{\ddagger}_{RC} \quad (23)$$

$$\Delta G_{CPE} = \Delta G_{0CPE} + S_{CPE}\Pi^* + A_{CPE}\alpha = (8.024 - 3.500\Pi^* - 1.610\alpha)\ \text{kJ mol}^{-1} \quad (24)$$

$$\Delta G^{\ddagger}_{RC} = \Delta G^{\ddagger}_{0RC} + S_{RC}\Pi^* + A_{RC}\alpha = (84.290 + 1.360\Pi^* + 22.842\alpha)\ \text{kJ mol}^{-1} \quad (25)$$

The signs of the parameters reinforce our conclusions concerning the solvent effects. In the case of CPE, the parameter Π^* is negative, similarly as predicted by the Kirkwood−Onsager model, and the parameter α is very small, indicating that CPE is practically independent of the HBD properties of the solvents. In the case of the RC step, Π^* is small and positive, as predicted earlier, while α is large as an indication of the significant effect of HB. The correlation between the theoretically computed and predicted $\Delta G^{\ddagger}_{TOT}$ values is good (Figure 14).

Table 8. Parameters and Their Errors (kJ mol^{-1}) for the Theoretically Calculated ΔG_{CPE} and $\Delta G^{\ddagger}_{RC}$ Values Obtained from the Kamlet−Taft Multilinear Regression[67,68]

	ΔG_0	error	Π^*	error	α	error	R^2
CPE	8.024	1.459	−3.500	1.769	−1.612	0.999	0.605
RC	84.290	3.362	1.360	4.121	22.842	2.074	0.986

(67) Kamlet, M. J.; Taft, R. W. *J. Am. Chem. Soc.* **1976**, *98*, 2886−2894.

(68) Konnors, K. A. *Chemical Kinetics: The Study of Reaction Rates in Solution*; Wiley & Sons: New York, 1990; Chapter 8.4, pp 442−446.

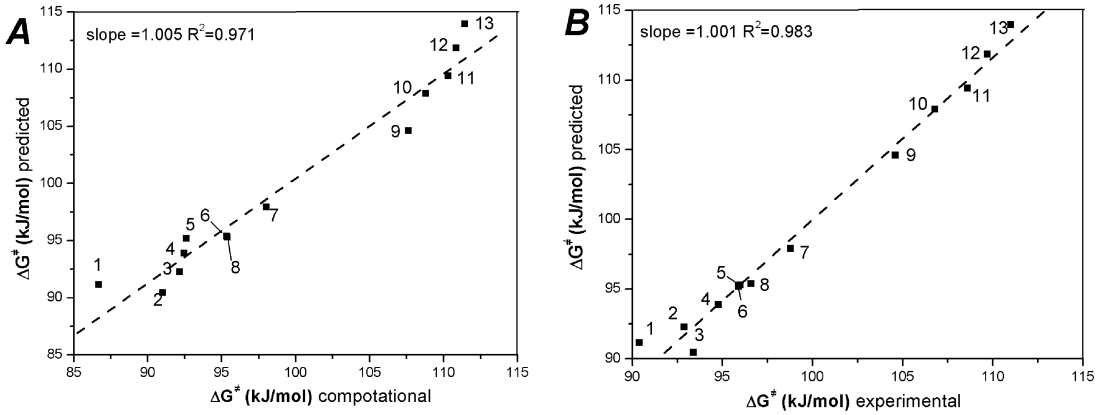

Figure 14. (A) Correlation between the theoretically computed ($\Delta G^{\ddagger}_{TOT}$; the sum of CPE and RC) and predicted values (A) and that between the experimentally measured ($\Delta G^{\ddagger}_{OBS}$) and predicted values (B) for the rearrangement of *N*-propargylmorpholine *N*-oxide **1** using parameters obtained from the multilinear regression (eqs 23−25) (see text). 1: Dioxane. 2: Pyridine. 3: Me_2CO. 4: MeCN. 5: Me_2SO. 6: $MeNO_2$. 7: $CHCl_3$. 8: CH_2Cl_2. 9: *t*-BuOH. 10: *i*-PrOH. 11: EtOH. 12: MeOH. 13: H_2O.

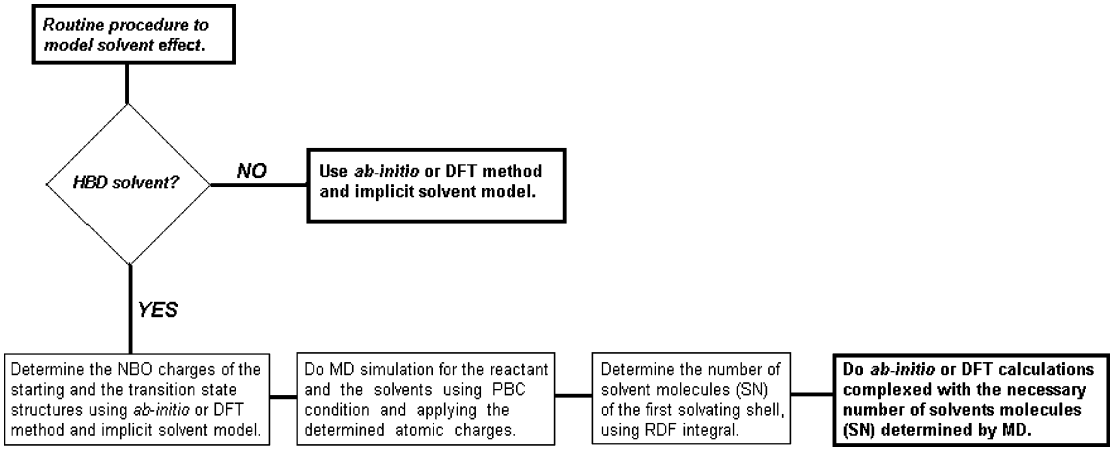

Figure 15. Schematic representation of the procedure applied for appropriate modeling of the solvent effects.

5. Conclusions

Our aims were to find an all-purpose way with which to predict the kinetic parameters of reactions in different solvents (Figure 15) and which would be useful for both general chemistry and preclinical development processes in the pharmaceutical industry. As demonstrated here, the exchange of aprotic solvents for protic ones can lead to great alterations in chemical processes as concerns both the mechanism and the reaction parameters. We have demonstrated that halogenated hydrocarbons form a distinct solvent group because they exhibit a weak but significant HBD ability in addition to aprotic behavior. The commonly used PCM solvent models are applicable for the modeling of aprotic solvents. When HB may occur and play a significant role, the number of solvating molecules can be determined by using MD simulations. Starting from this basis, the joint explicit−implicit solvent model gives accurate results.

Acknowledgment. The authors are grateful to Professor Ferenc Ruff for his interest and stimulating discussions. We thank Dr Lelle Vasvári-Debreczy and Dr David Durham for their assistance toward the linguistic improvement of this article. One of the authors (I.G.C.) wishes to thank the Ministry of Education for a Szent-Györgyi Visiting Professorship, and the Hungarian Scientific Research Fund for financial support (OTKA T046861). This article is dedicated to Professor András Lipták on the occasion of his 70th birthday.

Supporting Information Available: Explanation and details of experimental and theoretical methods used. Scheme S1: chemical structures of selected MAO inhibitors. Table S1: NMR chemical shifts of *N*-oxide **1** recorded in various solvents and at different temperatures. Table S2: the energy values of *N*-oxide **1** obtained by different computational methods. Table S3: the parameters of MD simulations. Tables S4−S45: kinetic raw data measured by NMR and GC. Figures S2−S43: evaluation of kinetic raw data and experimental errors. Tables S46−S49: equilibrium and transition state energies and ZPEs, together with the corresponding geometries in xyz files. Reference 42 in completed form. This material is available free of charge via the Internet at http://pubs.acs.org.

JA042227Q